Electrostatic Force Microscopy and Atomic Force Microscopy's Applications to Integrated Circuit Internal Signal Measurements

Richard Xuesong Qi

Department of Electrical and Computer Engineering
University of Manitoba
Winnipeg, Manitoba, Canada

A thesis submitted to
the Faculty of Graduate Studies
in partial fulfillment of
the requirements for the degree of

Master of Science

THE UNIVERSITY OF MANITOBA

FACULTY OF GRADUATE STUDIES

*****

COPYRIGHT PERMISSION PAGE

ELECTROSTATIC FORCE MICROSCOPY AND ATOMIC FORCE MICROSCOPY'S APPLICATIONS TO INTEGRATED CIRCUIT INTERNAL SIGNAL MEASUREMENTS

BY

RICHARD XUESONG QI

A Thesis/Practicum submitted to the Faculty of Graduate Studies of The University of Manitoba in partial fulfillment of the requirements of the degree of

Master of Science

Abstract

Measuring the signals at the internal nodes of integrated circuits is important for the design verification and failure analysis of advanced microelectronics. Technological breakthroughs in the evolution of the VLSI (Very Large Scale Integration) design and the microelectronic fabrication have continually driving integrated circuits to be denser, faster and more complicated. The internal signal testing of integrated circuit is a challenging problem for test engineers and researchers who must continually to develop new measurement techniques to keep pace with the technological advances. Electrostatic force microscopy has been demonstrated to be a viable technique to meet the challenge, and it is capable of performing non-invasive, high-spatial and temporal resolution, and high-speed integrated circuit internal signal measurements. This report presents a amplitude modulation high-speed non-contact signal sampling technique using electrostatic force microscopy. The report also introduces the atomic force microscopy and its application of sub-micron contact signal probing. Both techniques have been implemented and integrated into a reasonably practical probing system. Non-contact and contact measurements by this probing system on several test devices from commercial fabrications are performed, and the results are presented in this report. Based on the test result analyzed, the report concludes that the probing system, which utilizes the electrostatic force microscopy and atomic force microscopy techniques, is a reasonable tool for practical integrated circuit internal node testing.

Acknowledgments

First of all, I would like to express my deeply thanks to Dr. Doug Thomson and Dr. Greg Bridges for giving me the opportunity to research in such an innovative field, and for your supervision, your support and your kindness during the study. I felt so grateful that I had your help when I switched my academic field and when I started my industrial career.

I am grateful to everyone who contributed to this thesis. I would like to thank all members of SPM group, the department's technical staff at University of Manitoba, and my colleges at Micro Force Instruments, Inc. for their helps and contributions during this work.

Deeply thanks to my wife, Baini. Thanks for the endless love you give to me and all the happiness you created in our life. It was your support and encouragement being with me every step in the last ten years, during my academic studying and industrial career building. Your caring and understanding make me always feel that I have a peaceful harbor, our home, when I am tired outside. I know I am so much blessed to have you in my life.

Finally, I greatly thank my parents and my brothers in China. Their unconditional love have been supporting and encouraging me all the time.

This work was supported by the Natural Sciences and Engineering Research Council (NSERC), the Canadian Microelectronics Corporation (CMC), Micronet, and MFI Technologies, Inc.

Contents

List of Figures

List of Acronyms

ADC	analog-to-digital converter
AFM	atomic force microscope/microscopy
CMOS	complementary metal-oxide-silicon
DAC	digital-to-analog converter
DSP	digital signal processor
DUT	device under test
EFM	electrostatic force microscope/microscopy
FET	field effect transistor
FWHM	full-width half-maximum
GPIB	general-purpose interface bus
IC	integrated circuit
MFM	magnetic force microscope/microscopy
SFM	scanning force microscope/microscopy
SPM	scanning probe microscope/microscopy
SRM	scanning resistance microscope/microscopy
SRD	step recovery diode
STM	scanning tunneling microscope/microscopy
VLSI	very large scale integration

Chapter 1

Introduction

1.1 Motivation

Measuring the signals at the internal nodes of integrated circuits (ICs) is important for the design verification and failure analysis of advanced microelectronics. Technological breakthroughs in the evolution of the VLSI (Very Large Scale Integration) design and the microelectronic fabrication continually drive integrated circuits to be denser, faster and more complicated. The latest International Technology Roadmap for Semiconductors [1] from Semiconductor Industry Association suggests the emergence of microelectronic circuits with deep sub-micrometer or below 100 nanometer critical structure numbers, several GHz clock rates, and few hundred millivolts of operating voltage in the near future. This creates major challenges for test engineers and researchers in the IC failure analysis field who must continually develop new measurement techniques to keep pace with advances in microelectronics. As IC density, speed and complexity increase, information on internal signal's rising/falling times, delays, waveshapes and voltage-levels are required for characterizing potential dynamic failures. A technique to perform high

frequency, and non-invasive measurements at the internal nodes of an integrated circuit with high-spatial and accurate temporal resolution would be a useful IC failure analysis tool. In this report, the techniques based on scanning probe microscopy (SPM) are applied to IC internal signal measurements.

1.2 Outline

This report presents electrical probing methods of IC internal signal measurement using two SPM-based techniques, electrostatic force microscopy (EFM) non-contact high-speed sampling, and atomic force microscopy (AFM) sub-micron contact probing. This work includes the study of the characteristics of the two techniques, their implementation into a probing system, and their applications on several practical IC devices. Following this introduction, Chapter 2 reviews several alternative techniques for measuring IC internal node signals to provide the context for this work. Chapter 3 provides an overview of related SPM techniques, and its main part is focused on electrostatic force microscopy operating principle. Chapter 4 studies the theories and characteristics of the electrostatic force microscopy non-contact high-speed sampling, and the atomic force microscopy sub-micron contact probing techniques. The system architecture of their implementation into a probing system is reviewed. Chapter 5 presents IC internal signal measurement results of both laboratory test samples and commercial IC chips. Both non-contact and contact measurements are performed. Finally, Chapter 6 summarizes this study, draws several conclusions, and provides few suggestions for further research in this area.

Chapter 2

Review of IC Internal Testing Techniques

As the importance of IC internal testing and its commercial potential, many diagnostic tools have been developed to measure IC internal signals. This chapter offers an overview of some alternative techniques used in microelectronics testing. They are broadly divided into two categories: contact probing, and non-contact probing.

2.1 Contact Probing

Contact probing is the simplest way to measure a signal in an integrated circuit by establishing an electrical contact with a needle probe between the test point and test equipment. Depending on the applications and devices-under-test (DUT), various types of contact probes are used, and they are discussed in the next few sections.

2.1.1 On-wafer contact probing

Wafer probing is to test chips while they are still in semiconductor wafer. It is an especially critical production test. Wafer probing ensures that the chip manufacturer avoids incurring the significant expense of assembling and packaging chips that do not meet

specification by identifying flaws early in the manufacturing process. As each chip contains numerous bond pads, typical contact on-wafer probes have multiple probe tips, and they are arranged into a customized test fixture (called a probe card) so that probe tips can simultaneously contact all of the bond pads on one or maybe several chips. A Probe station is usually used to manually or automatically align the wafer to permit the probes to precisely contact the chip bond pads. Test equipment transmits electrical signals through the probes or probe card to the chip and evaluates the signals which return from the chip. Test equipment used with on-wafer contact probing in production test is often called automated test equipment, or ATE, and is designed specifically for high-volume testing.

2.1.2 Low Impedance Passive Probe

Low impedance passive probe is often used for monolithic microwave integrated circuit high frequency signal measurement. High frequency probes up to 220 GHz are commercially available [2]. Measuring at GHz frequencies requires controlling the probe impedance to match the characteristic impedance (usually 50Ω) as close as possible to the test point to minimize the parasitic inductive and capacitive effects. Microwave low impedance passive probe are commercially available in coaxial, microstrip and coplanar configurations [3]. As shown in Figure 2.1 (a) and (b), a coaxial probe is to extend the center conductor of a shielded coaxial cable to form the probe tip, and a micro strip probe is formed by attaching a short needle probe to the end of the microstrip feed line. Both of them can provide a 50Ω impedance match within a few millimeters to probe point. However, the main drawback of them is the parasitic inductance of the probe tips and the lack of RF ground signals close to the test point.

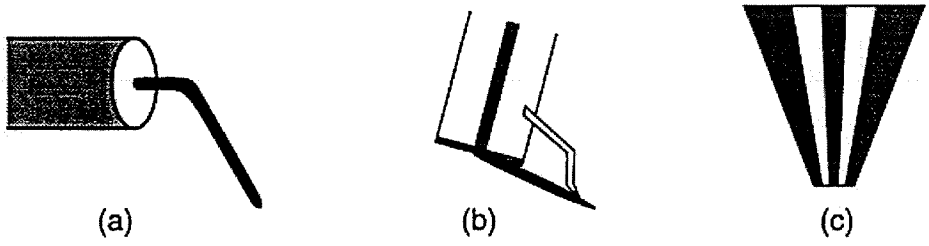

Figure 2.1 Microwave probe types: (a) Coaxial probe, (b) Microstrip probe, (c) Coplanar probe [3].

In a coplanar waveguide configuration, as shown in Figure 2.1 (c), the probe is practically the center signal line of a 50Ω transmission line. Probe signal line is located between two ground lines and geometries of them are designed so that characteristic impedance is 50Ω. The end of the line is tapered in width to match the probe point to the test pads on a test device. The use of a coplanar probe to test a high frequency GaAs FET (Field Emission Transistor) is illustrated in

Figure 2.2. Ground-Signal-Ground three direct contacts are made between coplanar probe tips and each set of test pad, and the other sides of coplanar probes are connected to a network analyzer to obtain S-parameters of the FET device.

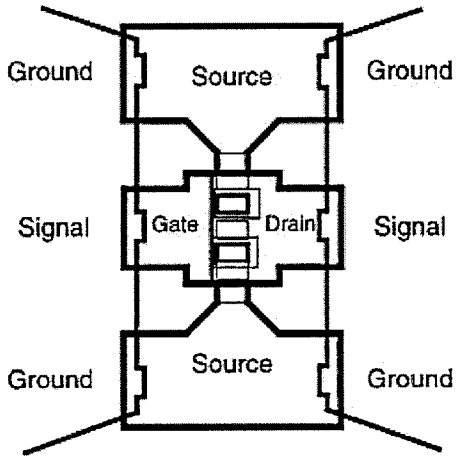

Figure 2.2 Measurement of a GaAs FET using two coplanar probes [33].

2.1.3 Resistive divider passive probes

Resistive divider probes are examples of passive medium impedance probes. For example, a 450Ω resistor is inserted in the signal line of the probe tip, and it results in a 10:1 attenuation and input impedance of 500Ω in a 50Ω system. The measurement bandwidth of resistive divider probes ranges from DC to 10GHz [4]. Probe input impedance can go up to 5kΩ or higher. However, as the signal attenuation gets larger the signal becomes more difficult to measure. This medium resistive loading and larger capacitive loading are important limitations of these probes.

2.1.4 Active high impedance probes

Active probes are designed to achieve very high input impedance and very small capacitive loading to the test point. The probe tip is directly connected to the unprotected gate of a MOS field effect transistor (FET), and the MOS FET acts as a buffer between the probe needle and a matched impedance transmission line. The active probes usually have a loading of 0.01pF to few pF, which is mostly the gate capacitance of the MOS FET. For example, a commercially available active probe from Picoprobe [2] has an input capacitance load of 0.04pF and a DC to 1 GHz 3-dB bandwidth. In order to achieve a large measurement bandwidth it needs to increase the coupling capacitance between the test point and measurement system, but this will also increase the effective capacitive loading. There is usually a trade-off between bandwidth and loading.

2.2 Non-Contact Probing Techniques

2.2.1 Electron beam testing

Electron beam testing equipment has been commercially available and widely utilized as IC internal signal measurement tool by the microelectronics industry for the past two decades [6]. The principle of electron beam testing technique may be described with reference to Figure 2.3, which shows schematically an electron beam focused onto an IC conductor.

Where the primary electron beam impinges, low-energy secondary electrons are released from the IC conductor's surface, with an energy distribution function characteristic of the emitting secondary electrons, as shown in Figure 2.3 (a). If a voltage is applied to the conductor, the secondary electrons lose or gain proportional amount energy, which translates to a shift in their energy spectrum. For emission with positively biased conductor, as shown in Figure 2.3 (b), lower energy secondary electrons are trapped by local potential or reflected by a retarding field in an energy analyzer. This reduces the detected por-

tion of the spectrum. Analyzing the detected secondary electron spectrum gives localized voltage information at test point.

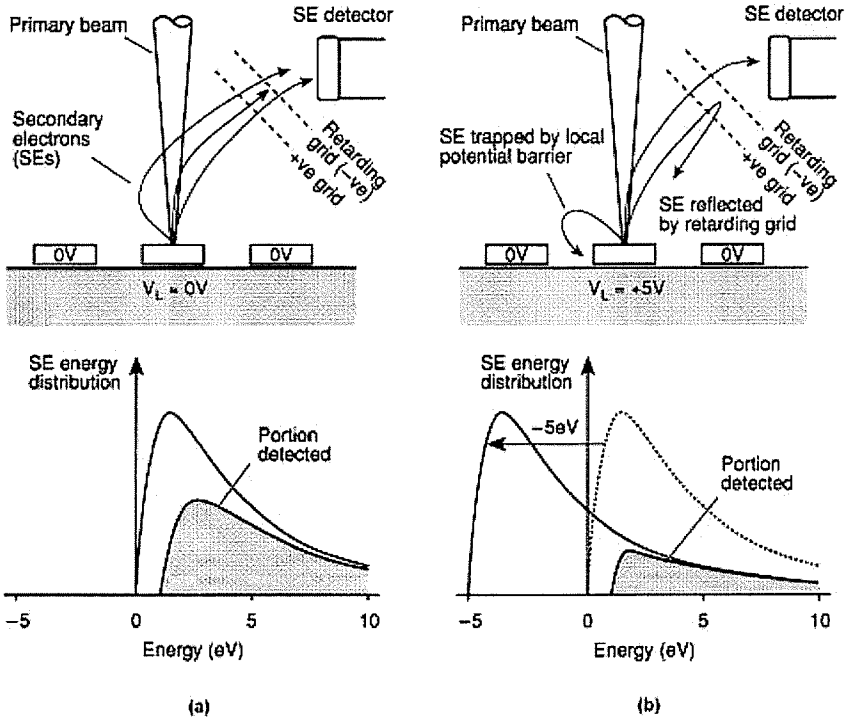

Figure 2.3 Principle of electron beam testing technique. (a) Conductor being probed biased at 0V. (b) +5V bias on conductor and accompanying shift of secondary electron energy distribution [6].

High frequency measurement is achieved by using a pulsed primary electron beam, and an equivalent-time scale sampling technique is used. The electron pulses are synchronized with the repetitive circuit signal, and the signal amplitude at pulse location on an equivalent-time scale is measured by examining the detected SE energy spectrum. By shifting the sampling pulse's phase relative to the repetitive signal, the waveform can be constructed point by point.

For low energy electron beam, the electron beam testing is non-invasive to normal circuit operation. Several GHz of measurement bandwidth, voltage sensitivity of $160mV/\sqrt{Hz}$, and below 0.5μm spatial resolution are achieved [7]. The frequency capability of electron beam testing is limited at about 8GHz due to the primary electron sampling pulses of about 40ps and the transit time effect of the secondary electrons [8]. Electron beam

testing system is complex and expensive since measurement has to be done in a vacuum. Devices under test must be placed in the vacuum and the electrical interface has to be made through this vacuum between the devices and outside circuit stimulus system and measurement equipment.

2.2.2 Photoemission probing

Photoemission probing of ICs relies on the detection and analysis of the weak light pulses that are emitted by field-effect transistors (FETs) during their switching operations. Figure 2.4 depicts the switching current induced light emission at FETs gates of a CMOS inverter. Under static conditions, where the p-FET is fully conducting and n-FET is switched off (while input voltage equals zero) or where the p-FET is switched off and n-FET is fully conducting (When input voltage equals Vdd), there is no current flowing in the FETs. On the other hand, when this inverter is changing its logic state, a transient current does flow through the FETs, and it leads to a transient emission of light. Photoemission probing uses this effect to obtain IC internal signals' timing information. For example, by detecting the emitted light pulses from different logic cells in a circuit and analyzing the timing difference between the pulses will provide delay information between these logic elements.

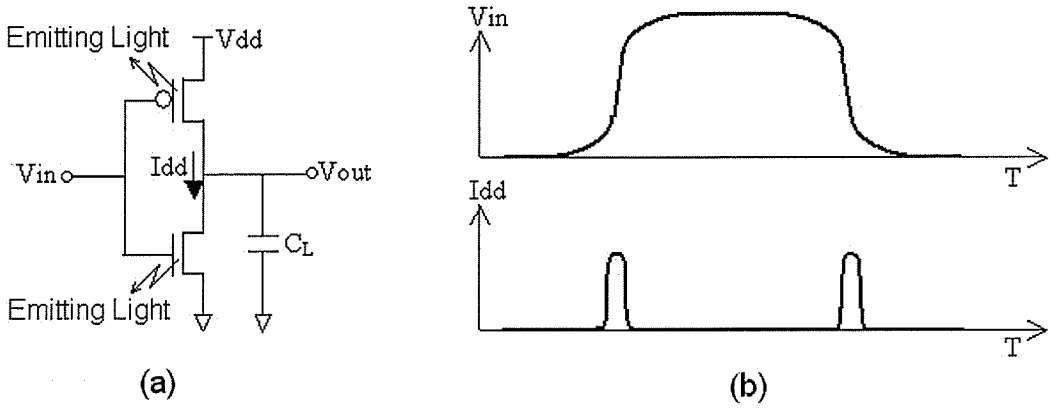

Figure 2.4 (a) Light emission from FETs' gate areas induced by transient current of a CMOS inverter. (b) Diagram of CMOS FET's transient currents of a inverter.

Using a time-correlated photon counting technique [9], The temporal properties of light detected by photon counting can be analyzed at the picosecond level. A spatial resolution of 1μm was achieved by using a Mepsicron photon detector [10]. It works with high magnification optical system on the photo-cathode of the photon detector. This technique is also able to probe several test points in the same time as light emissions can be detected simultaneously.

A big disadvantage of this technique is that the measurement may be very time-consuming. As experimentally discovered [11], a detectable photon emission usually only happens in 1 of 10^6 switching operations, photon detector system integration times can approach hundreds of thousands of seconds in the worst case, or as long as 10 to 20 hours. This is the case particularly when the repetition rates for the test patterns used to exercise a chip can be of the order of microseconds or longer.

2.2.3 Electro-optic sampling

This technique employs the electro-optic effect [12] that is the change in the birefringence properties of certain crystals when placed in an electric field. This effect rotates the polarization of light propagating through such a crystal. An electro-optic probe can be constructed with such electro-optic crystal, typically $LiTaO_3$, at probe tip, as shown in Figure 2.5.

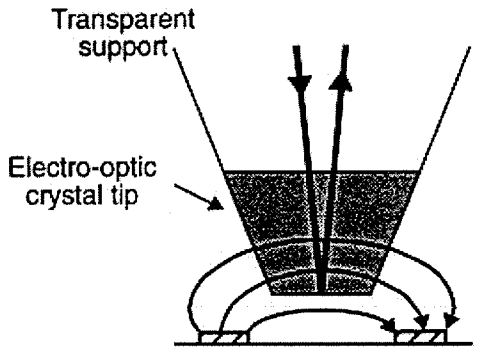

Figure 2.5 Diagram of electro-optic sampling probe tip.

The probe is positioned close to the test point, and the tip end is emerged in the electrical field to be tested. An optical beam travels in the probe through the electro-optic crystal tip, and it is reflected by the end of probe tip. By measuring the polarization change of the reflected beam, the electric field resulting from voltages on a circuit can be investigated.

The principle of a more detailed electro-optic probing setup is depicted in Figure 2.6. A Laser is focused into the electro-optic probe and is reflected back by the probe end mirror surface. The use of polarizing beam splitter and the photo-detector enables the measurement of polarization changes of the return Laser beam, and the changes are directly related to the electrical signals at test point. Normally measurement of high-speed signals needs a sampling technique where the Laser beam is a train of short pulses and they are the sampling gates. This sampling technique requires the signal to be measured is repetitive. The pulse width of the Laser beam determines the temporal resolution of this measurement technique. Advances in Laser technology have enabled the generation of very short pulses, as low as 100fs in some of the fastest systems [12], which provides a very high temporal resolution.

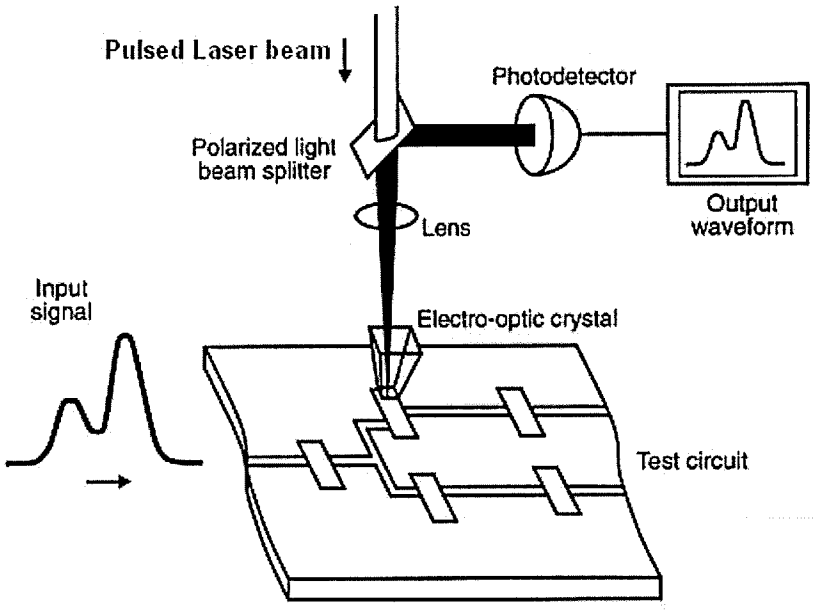

Figure 2.6 Diagram of electro-optic probing setup.

Electro-optic probing is expected to have very minimal invasiveness due to the carrier generation by the Laser light. It has excellent temporal resolution as long as very narrow Laser pulses can be generated, however it is complex and expensive equipment due to the complexity of Laser system. As the technique measures the electric fields instead of the voltage directly, calibrations are required for absolute voltage measurements.

2.2.4 Infrared Laser probing

Infrared Laser diagnostic system is optical probing equipment that mainly developed for flip-chip backside probing. Backside probing is measuring IC internal signals from the silicon substrate side for flip-chip mounted ICs, and it will be explained in details at later section. In operation, the system uses infrared lasers operating at 1.06 microns to probe through the backside of devices. At that wavelength, silicon of even 800-micron thickness is transparent to infrared light, thus eliminating the need to produce deep holes in an IC to access the active regions of CMOS transistors. This technique relies on the interaction between the optical beam and the local electrical field generated by the IC transistor switching operations. The variation in carriers between source and drain during transistor switching produces an electrical field, and this field can vary the phase and amplitude of a light beam reflecting from the device. For high-speed measurement, a pulse sampling technique is used. The infrared Laser generates a train of sampling pulses that are synchronized with circuit excitation signals. Examining the reflected beam's phase and amplitude changes gives the signal timing information at switching transistor.

Besides its backside probing capability, the infrared Laser probing system is also non-invasive electronically to the circuit under test. Measurement bandwidth of 10GHz and timing resolution of 10ps are achievable [13]. However, focusing of the infrared Laser limits this technique's special resolution to about 0.5μm. Since the test points have to be active areas of IC transistors, this technique is not good to test signals at IC metal conductors.

Chapter 3

Electrostatic Force Microscope

Having reviewed several alternative methods for IC internal signal measurement, this chapter will focus on the technique we used for the task the Electrostatic Force Microscopy (EFM). Since the invention of scanning tunneling microscope (STM), various forms of scanning probe microscopy (SPM) techniques were developed. They all measure certain localized properties of a sample using interaction with a very sharp probe operated very close to its surface. EFM is one member of SPMs, and the interaction between an EFM probe and test sample is, as its name says, electrostatic force. EFM is capable of measuring a sample's surface properties that affect the electrostatic interaction, such as surface charge density, surface potential. This chapter discusses EFM's operating principle. It starts with brief introductions of STM, as STM is the origin of all SPM techniques. A broad review is given to a subset of SPM, which is scanning force microscopy (SFM). Finally, the EFM operating principle is presented in details.

3.1 Scanning Tunneling Microscopy

Scanning Tunneling Microscopy was invented by Gerd Binnig and Heinrich Rohrer in 1982 [14]. It enables surface topography measurements with atomic resolution for the

first time, and Gerd Binnig and Heinrich Rohrer were awarded Nobel Prize for their remarkable achievements.

A sample STM operation illustration is shown in Figure 3.1. A sharp metallic tip is brought close to a conducting substrate at a distance of few Angstroms. At this distance, there is a significant overlap between the electron wave functions of the atoms in the very tip end and substrate right below it, and the space between the tip and substrate plays the role of a potential barrier. When a bias voltage is applied between the tip and the substrate, a tunneling current is established through this potential barrier. Using a square potential barrier approximation, the tunneling current decays exponentially within the barrier, so it often flows between few atoms or even a single atom at very end of the sharp tip and a localized atom cluster in substrate surface. This property gives STM the ability for atomic resolution surface studies.

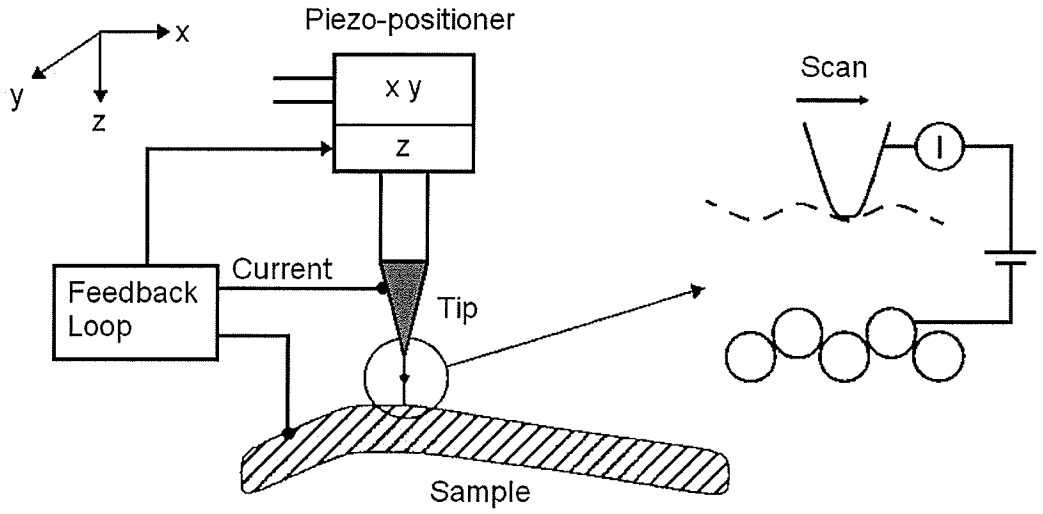

Figure 3.1 Schematic of the scanning tunneling microscopy technique [14].

As seen in Figure 3.1, the motion of the tip is controlled on a fine scale by a piezoelectric positioner. STM is usually operated in a constant current mode using a feedback loop. The feedback loop sends control signal to the piezo-positioner Z-axis and causes the tip to track the substrate surface with very high precision while it is scanned over the sample. Thus the Z-direction control signal provides the surface topography data.

Measurements with STM can only be performed on metallic surface, and both the tip and sample have to be conducting. However, the success of the initial STM experiment has conceptualized a whole new set of scanning probe microscopes that are used in surface physics, material science, biologic studies, and many other fields.

3.2 Scanning Force Microscopy

Scanning force microscopy (SFM) is the technique that was stimulated by the STM principle concept. Like in a STM, the same sharp tip and precise tip motion control mechanism are used, however a scanning force microscope employs the force between the tip and the sample surface instead of tunneling current. Thus, SFM overcomes the limitation of the STM which is the need for conducting tip and test surfaces. In order to monitor the force, as shown in Figure 3.2, a scanning force microscope's sharp tip is usually mounted at the end of a small, flexible cantilever beam, and the cantilever deflection is measured, which is proportional to the force acting on the tip. Structures and characteristics of SFM tip and cantilever are going to be reviewed in details later in this chapter.

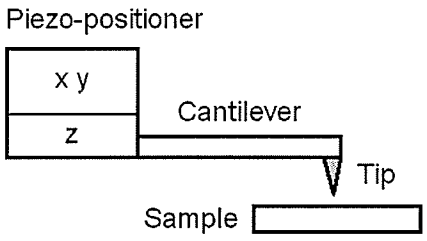

Figure 3.2 Diagram of scanning force microscopy operating principle.

Various SFM tools were developed according to different characterizations of the force between the tip and the surface. Atomic force microscopy (AFM) was the very first one [15]. In an AFM tool, the AFM's sharp tip is placed in contact with the surface of the material under investigation. The designated contact force is typically the repulsive atomic interaction which results from the overlapping of electron clouds of the atoms around the contact points between the tip and the surface. As the tip is scanned over the

sample surface, the atomic force deflects the cantilever. Similarly, a feedback system can be used to keep a constant repulsive force with controlling a steady deflection of the cantilever. In the mean time, the tip is scanned over the sample to track the topography of the surface. AFM surface imaging resolution at the order of nanometer is achievable with very sharp tips.

The AFM contact-mode surface micro-imaging concept has been extended beyond just obtaining surface topographies. For example, the Scanning Capacitance Microscope (SCM) [16] and scanning resistance microscope (SRM) [17] are contact microscopes that are able to perform 2-D profiling of carrier and dopant concentrations in semiconductors with nanometer spatial resolution. SCM and SRM measure localized contact capacitance and resistance, which are related to local semiconductor carrier and dopant concentrations, to trace dopant levels in semiconductor devices. Both the SCM and SRM are very useful tools for the verification of integrated circuit fabrication processes.

SFMs operated in non-contact mode have also been developed to minimize the contact disturbance to samples under test. With non-contact SFMs, the tip and the sample surface are at relatively large separation, usually beyond 10-100 nm. At this distance, the interactions between the tip and the surface are dominated by long-range forces, and they are typically Van Der Waals, Coulomb, magnetic, and electrostatic forces. Since these long - range forces are usually much smaller than contact forces, the force detection technique is different from measuring cantilever defection directly. Instead, the force gradient detection technique is often used. The cantilever is driven by an exciting signal at a frequency close to its resonant frequency. Due to interactions between the tip and the sample, the force gradient on the tip is like add or subtract of a spring and changes the resonant frequency of the cantilever, as seen in Figure 3.3. The shift in resonance can be detected by observing the change amplitude of the cantilever vibration. Techniques which measure phase and frequency changes of the cantilever are also used to examine the long-range tip-surface forces.

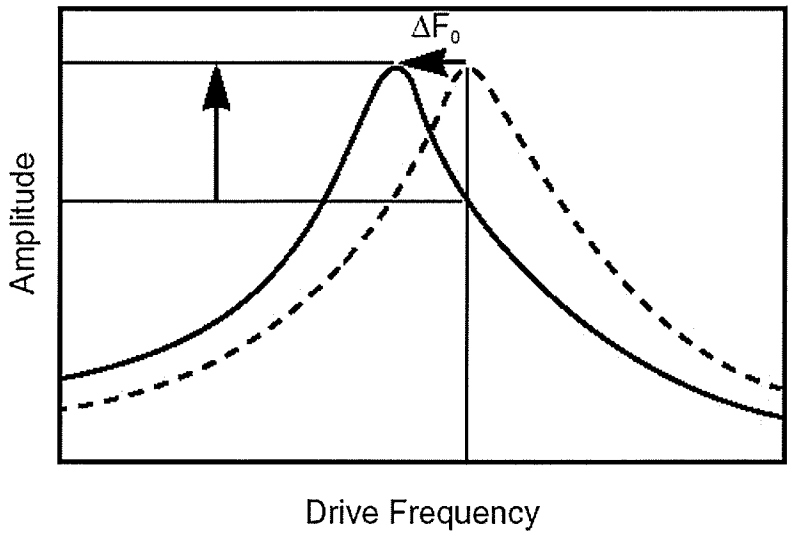

Figure 3.3 Diagram illustration of measuring amplitude in force gradient detection technique.

Magnetic Force Microscope (MFM) is one of non-contact SFMs which uses a magnetic tip to detect magneto-static forces [18]. The tip is usually iron or nickel for their strong magnetic dipole moments. MFM can image topography and magnetic domains in a wide range of materials, such as magnetic recording medium which produces strong stray magnetic fields. Imaging spatial resolution is determined mainly by the sharpness of the tip and it can be as high as 10nm. An interesting application of MFM is internal current probing of integrated circuits [19]. This application utilized Ampere's law, and the magnetic fields which are generated by the electrical currents are imaged by scanning a magnetic tip over the conductor carrying the current. Current directions and magnitudes were examined from the images with reported sensitivities of 1mA DC and 1μA AC [19].

Electrostatic force microscopy technique, which utilizes the electrostatic force between the tip and samples, is the main focus of the research report. EFM has been developed for microelectronics test applications, such as: measuring the localized surface charge [20], profiling semiconductor carriers [21], imaging ferroelectric domains [22], and examining the contact potential difference between various types materials [23]. This research work employs EFM to IC internal signal probing. EFM principle is presented in the following sections.

3.3 Electrostatic Force Microscopy

3.3.1 Basic operation principle

An EFM instrument operates by detecting the cantilever deflection of a small conducting probe which is caused by the electrostatic force between the tip at the end of the probe and the integrated circuit under test. The electrostatic force results from the potential difference and the capacitive coupling between the probe and the circuit under test. Figure 3.4 illustrates an EFM probe tip is placed at a small distance above a conductor trace of a test sample.

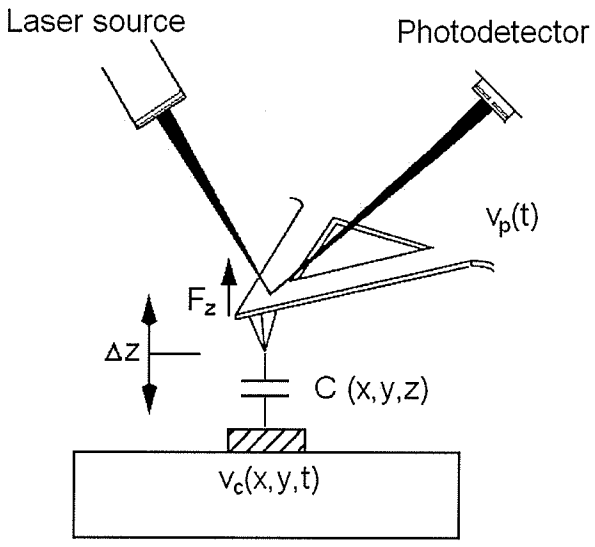

Figure 3.4 Electrostatic force microscopy operating principle.

The conducting EFM probe is excited at a specified voltage $v_p(t)$, and localized voltage of the conductor trace is $v_c(x,y,t)$, which is the unknown voltage and to be measured. The EFM tip and the conductor also form a localized capacitance $C(x,y,z)$. As the electrical energy of the capacitive system can be expressed as:

$$U = \frac{1}{2} CV^2 \tag{3.1}$$

then, the electrostatic force experienced by the EFM probe is:

$$F = \nabla U = \frac{1}{2}\nabla(CV^2) \tag{3.2}$$

Due to EFM cantilever's geometry, the main deflection of it is at z-axis, and EFM deflection sensor is also configured to detect z-direction deflection. Z-axis electrostatic force is given by:

$$F_z = \frac{1}{2}\frac{\partial}{\partial z}(CV^2) \tag{3.3}$$

Replacing the capacitance and voltage difference between the capacitor by notations shown in Figure 3.4, (3.3) becomes:

$$F_z = \frac{1}{2}\frac{\partial}{\partial z}C(x, y, z)[v_p(t) - v_c(x, y, t)]^2 \tag{3.4}$$

According to above equation, the electrostatic force is proportional to the capacitance gradient which is dependent on the localized physical geometry and relative position of the EFM probe tip and the test sample; and the electrostatic force is also changing with the square of the potential difference between the probe and the circuit trace.

By sensing the deflections of the EFM cantilever induced by the force expressed in (3.4), information about the circuit signal $v_c(x,y,t)$ can be obtained. The next few sections will provide detail studies of the EFM cantilevers, EFM probe piezo-scanner's properties, and the cantilever deflection detection mechanism. They are all critical elements to EFM operation. Techniques to measure DC and analog circuit signal will also be reviewed.

3.3.2 EFM cantilever characterization

The EFM cantilever deflection by the electrostatic force relies on its mechanical properties. The cantilever acts as a spring, and its spring constant and frequency response are essential properties in EFM operation.

Spring constant k of a cantilever structure fixed on one end, defines the rigidity of its vibration, and is given by [24]:

$$k = \frac{3EI}{l^3} \tag{3.5}$$

Where l is the length of the cantilever, E is the modulus of elasticity, and I is moment of inertia. E is dependent on the material composition of the cantilever and I is a function of the cantilever geometries. For instance, a cantilever beam with a rectangular cross section of width w and thickness t has a moment of inertia $I=wt^3/12$. Then, the spring constant of this cantilever is:

$$k = \frac{Ewt^3}{4l^3} \tag{3.6}$$

As the electrostatic force is a function of time, the deflection of the cantilever under such force is defined by its dynamic response. Resonant frequency is a important parameter to determine the system dynamic response. A vibrating system has propensity to vibrate at a particular frequency, and this frequency is called the resonant frequency. By solving the homogeneous equation of the cantilever system, the fundamental resonant frequency of the above rectangular-cross-section cantilever, f_r, is given by [24]:

$$\omega_r \approx \sqrt{\frac{k}{0.24\rho wtl + m_{Tip}}} \quad \omega_r = 2\pi f_r \tag{3.7}$$

where k is the spring constant, p is the mass density of the cantilever material, and m_{Tip} is the mass of the tip only. Then result of the homogeneous equation of the cantilever motion under an external force, i.e. the frequency response, is [24]:

$$|G(\omega)| = \frac{(Q/k)(\omega_r/\omega)}{\sqrt{1+Q^2(\frac{\omega_r}{\omega}-\frac{\omega}{\omega_r})^2}} \quad \omega > 0 \tag{3.8}$$

This frequency response is graphed in Figure 3.5.

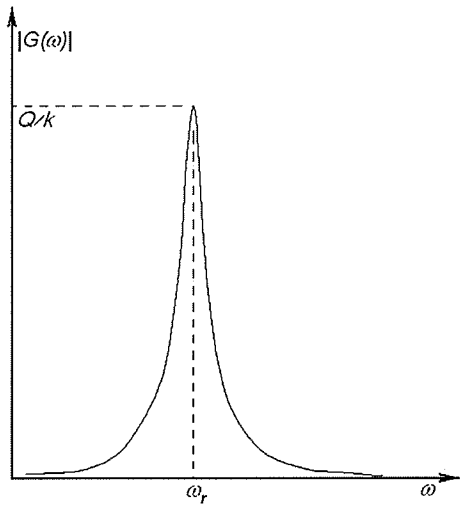

Figure 3.5 Data curve of the frequency response of the micro-machined rectangular cantilever.

where is Q is called quality factor, and it is defined as $\omega_r/\Delta\omega$ with $\Delta\omega$ being the 3dB bandwidth from resonance. Then cantilever deflection due to the external force F_z is:

$$\Delta Z(\omega) = F_z(\omega)\left|G(\omega)\right| = F_z(\omega)\frac{(Q/k)(\omega_r/\omega)}{\sqrt{1+Q^2(\frac{\omega_r}{\omega}-\frac{\omega}{\omega_r})^2}} \quad \omega > 0 \tag{3.9}$$

At $\omega=0$, equation (3.9) becomes $\Delta Z = F_z/k$, which is the static response of the system. It is the familiar Hook's Law.

As seen in Figure 3.5, with a normalized amplitude of external force, the maximum cantilever deflection occurs when the external driving frequency equals the resonant frequency. That is:

$$\Delta Z\big|_{\omega=\omega_r} = \frac{Q}{k}F_z(\omega_r) \tag{3.10}$$

Obviously, the magnitude of deflection at ω_r is enhanced by a factor of Q from that at static where $\omega=0$. As mentioned, the long-range electrostatic force is much smaller than the contact atomic force, and an EFM probe is usually driven at its resonant frequency to increase the sensitivity of the deflection detection.

The EFM probes used in this research are micro-machined cantilevers. As shown in Figure 3.6, they are silicon cantilever with W_2C conducting coating [25].

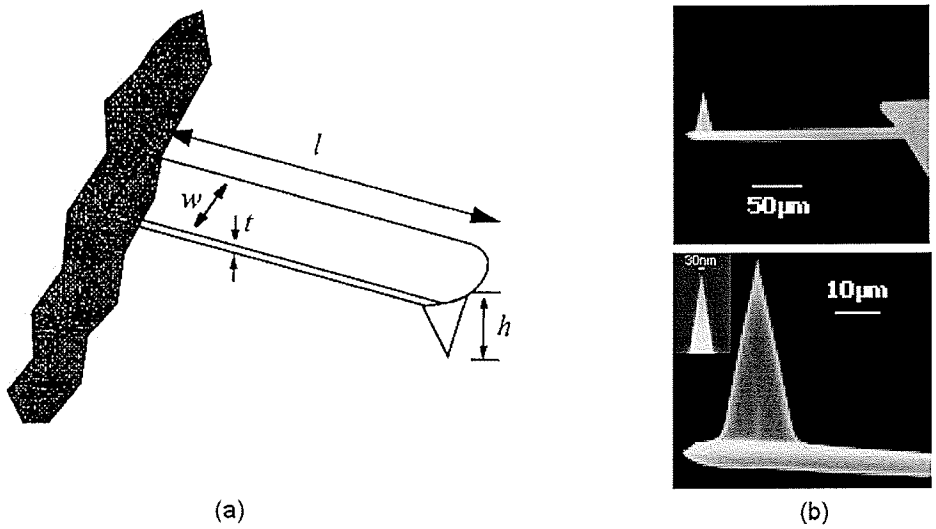

Figure 3.6 Micro-machined rectangular cantilever and tip.

Micro-machine technology is of utmost importance for fabricating EFM probe. As illustrated in Figure 3.6 (b), it is capable of fabricating probe tip with radius of curvature as small as 10nm. This is essential to achieve high spatial resolution for both contact imaging and non-contact EFM probing.

Typical geometries, spring constant, resonant frequency and Q factor [4] of these silicon rectangular cantilevers are listed below, which are from the data sheet of [25]:

Geometry:	l=350±5μm, w=35±3μm, t=1.5±0.2μm.
Spring constant:	0.05±0.02 N/m.
Resonant frequency:	14±3 kHz.
Q factor:	30±3.

3.3.3 Piezo positioner/scanner

EFM tools, like other SFMs, uses piezo actuators for very-high-resolution positioning and scanning. The actuators are made from elements of materials exhibit the piezo effect and change their dimensions under an applied electric field. As the displacement of a

piezo element is based on the continuously changing the orientation of electrical dipoles in the elementary piezo cell, its movement resolution depends on the electrical field applied and is theoretically unlimited. No one has yet observed quantum motion in piezo. Infinitesimally small changes in operating voltage are converted to linearly fine movements. To give a quantitative picture, as shown in Figure 3.7 (a), a PZT (Lead Zirconate Titanate, a common piezo material) tube with a 100V applied between inner and outer coating electrodes can reach a relative length change of 0.05%, that is 25μm for a 5cm long piezo tube. In another word, it moves 2.5 $\mathring{A}$ (about the size of an atom's diameter) by one millivolt.

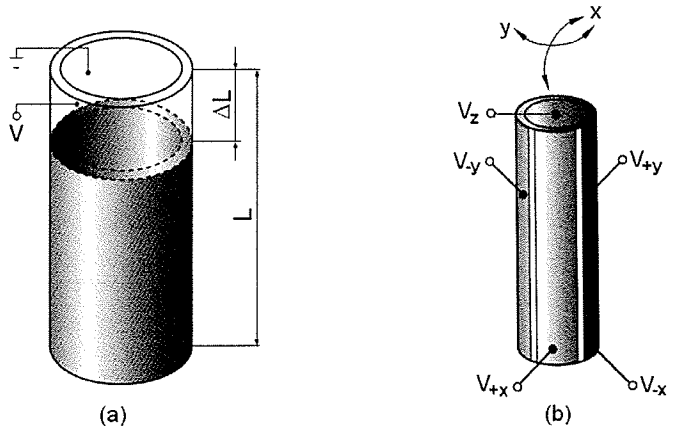

Figure 3.7 Piezo tube actuator and piezo tube scanner.

Figure 3.7 (b) also shows a sample 3-axes piezo scanner made by dividing the outer electrode into four parts. This scanner is able to distort the tube and move a sample mounted atop it in three dimensions by applying the appropriate voltages to the electrodes, and it is commonly used in laboratory scanning microscopes.

3.3.4 Laser beam deflection detection system

Laser beam deflection detection technique is a capable and reliable cantilever deflection method. It is widely used in various kinds of SPMs. The method is illustrated in Figure 3.8, where a Laser beam is focused on the end of the cantilever probe and reflected back to a bi-cell photodiode. The deflection of the cantilever causes the Laser spot movement

between two photoactive cells, then the difference of photocurrents induced by the Laser light between the two cells are converted to electrical signals. The following is a more detailed analysis.

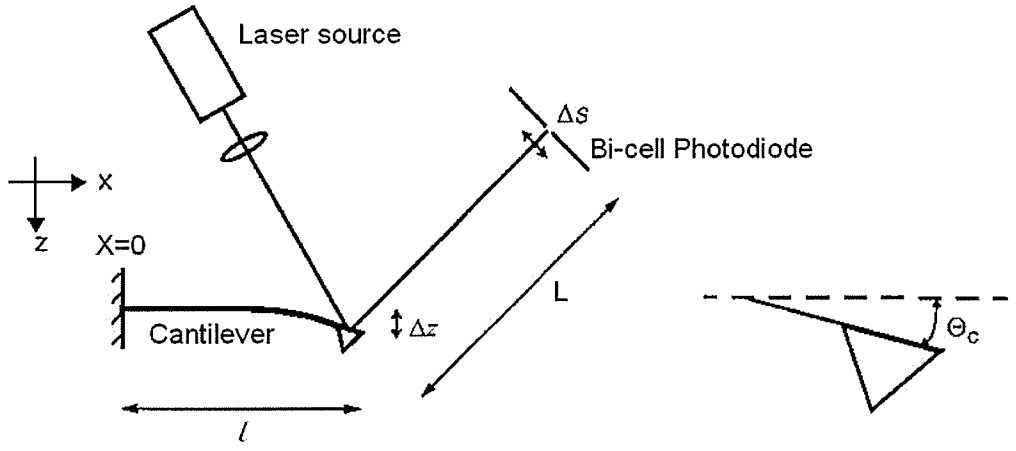

Figure 3.8 Laser beam deflection detection system.

The deflection along the cantilever due to a vertical force (F) applied at the end of it is given by:

$$z(x) = \frac{F}{6EI}(3lx^2 - x^3) \tag{3.11}$$

Where l is the length of the cantilever, E is the modulus of elasticity, and I is the moment of inertia of the cantilever. If the deflection is small, the deflection angle Θ_c at the end of cantilever can be approximated as following:

$$\Theta_c \approx \left.\frac{dz}{dx}\right|_{x=l} = \frac{Fl^2}{2EI} \tag{3.12}$$

Using (3.5) and $F=k\Delta z$, above equation becomes:

$$\Theta_c \approx \frac{3\Delta z}{2l} \tag{3.13}$$

Let Δs be the Laser spot displacement when the end of the cantilever is deflected from 0 to Δz. Therefore, using similar small angle approximation ($\Delta s << L$) and optical reflection law, Δs can be given:

$$\Delta s \approx \frac{3\Delta z L}{2l} \tag{3.14}$$

A bi-cell photodiode is used to detector this movement, as shown in Figure 3.9.

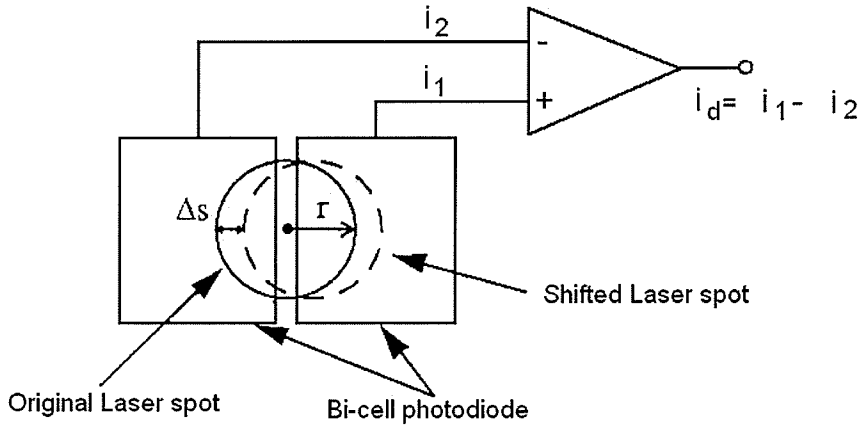

Figure 3.9 Diagram of bi-cell photodiode, and its generation of photocurrents.

A photodiode absorbs optical energy falling on it and generates a photocurrent. The current density, $j(x,y)$, at a given location of photodiode surface is:

$$j(x,y) = j_d + R_p E(x,y) \tag{3.15}$$

where j_d is dark leakage current density, R_p is the photo-responsivity of the photodiode material, and $E(x,y)$ is the incoming light energy density.

The Laser output power P_L is a fixed value (1mW in equipment used in this research). As a reasonable first order approximation, assuming Laser power is even distributed in the spot with a radius of r and separation of the two photo diode cells is small compared to r, the photocurrent difference, i_d, between two photo-cells when reflected beam moves Δs is then given by:

$$i_d \approx \frac{4R_p P_L}{\pi} \frac{\Delta s}{r} \tag{3.16}$$

Using (3.14) and substituting for Δs, we obtain:

$$i_d \approx \frac{6R_p P_L}{\pi} \frac{L\Delta z}{lr} \tag{3.17}$$

Thus the output signal i_d, the photocurrent difference in equation (3.7), from Laser deflection detection system is linearly proportional to the cantilever deflection Δz.

The noise generated by a photodiode is a combination of shot noise, due to the dark leakage current, and Johnson noise due to the shunt resistance of the device and the ambient temperature, and a typical sensitivity of the beam bounce detection sensor is report as $7.9\times10^{-6} nm/\sqrt{Hz}$ [26].

3.3.5 EFM Voltage Measurement Schemes

This section theoretically reviews EFM voltage measurement methods for DC and sinusoidal signal so that some electrical modulation and detection techniques are introduced.

3.3.5.1 DC Measurement

In a DC measurement, the electrostatic force, using equation (3.4), can be written:

$$F_z = \frac{1}{2}\frac{\partial}{\partial z} C(x,y,z)[v_p(t) - v_c(x,y) - \Delta\phi(x,y)]^2 \tag{3.18}$$

where $v_c(x,y)$ is the DC voltage on the circuit conductor, and $\Delta\phi(x,y)$ is the offset voltage due to surface charging or work function offset. As it is hard to accurately measure the electrostatic force and the capacitance gradient, a method, called force-nulling technique [27], is implemented by driving the probe with the following signal:

$$v_p(t) = A + K\cos(\omega_p t) \tag{3.19}$$

It is a cosine signal with amplitude of K and angle frequency of ω_p, plus a DC offset A. Substituting above probe signal into (3.18), we get:

$$\begin{aligned} F_z &= \frac{1}{2}\frac{\partial}{\partial z}C(x,y,z)[A + K\cos(\omega_p t) - v_c(x,y) - \Delta\phi(x,y)]^2 \\ &= \frac{1}{2}\frac{\partial}{\partial z}C(x,y,z)\left\{\{[A - v_c(x,y) - \Delta\phi(x,y)]^2 + \frac{K^2}{2}\}\right. \\ &\left. + 2K[A - v_c(x,y) - \Delta\phi(x,y)]\cos(\omega_p t) + \frac{K^2}{2}\cos(2\omega_p t)\right\} \end{aligned} \tag{3.20}$$

This equation suggests that the electrostatic force has a DC component which results in a static deflection of the cantilever as well as components at frequency ω_p and $2\omega_p$. As mentioned earlier the cantilever deflection amplitude is enhanced by a factor of Q if it is excited at its resonant frequency. Thus the signal-to-noise performance of the system is improved by choosing $\omega_p=\omega_r$, where ω_r is the cantilever resonant frequency. A lock-in-amplifier is also provided a reference at the same frequency so it will measure the deflection signal amplitude only at this resonant frequency. The cantilever deflection ω_r term is given by:

$$\Delta z\big|_{\omega_p=\omega_r} = \frac{Q}{k}F_z = \frac{Q}{k}\frac{\partial}{\partial z}C(x,y,z)[A - v_c(x,y) - \Delta\phi(x,y)]K\cos(\omega_r t) \tag{3.21}$$

The nulling technique is to adjust the value of A so that this amplitude is nulled. At this point, the localized surface voltage, $[v_c(x,y) + \Delta\phi(x,y)]$, equals A.

3.3.5.2 Sinusoidal Signal Measurement

Sinusoidal signals are base terms of all periodic signals. Usually an analog integrated circuit can be well characterized by its response of sinusoidal signals. This response measurement is very helpful to high-speed analog IC testing. Using EFM's non-linear relationship between the electrostatic force and the voltage difference, a mixing technique [28] and [29] can be employed to down-convert a high frequency signal to a lower frequency at which the EFM probe can respond with a measurable deflection. In this modulation scheme, the circuit signal and the sampling signal are as follows:

$$v_c(t) = V_c \sin(\omega_0 t + \phi_c) \tag{3.22}$$

$$v_p(t) = [A + K\cos(\omega_r t)]V_c \sin(\omega_0 t + \phi_p) \tag{3.23}$$

Using equation (3.4), the electrostatic force is given by:

$$\begin{aligned} F_z &= \frac{1}{2}\frac{\partial}{\partial z}C(x,y,z) \\ &\{[A + K\cos(\omega_r t)]V_c \sin(\omega_0 t + \phi_p) - V_c \sin(\omega_0 t + \phi_c) - \Delta\phi(x,y)\}^2 \end{aligned} \tag{3.24}$$

This produces a DC component as well as component at following frequencies: ω_r, $2\omega_r$, ω_0, $2\omega_0$, $\omega_0 \pm \omega_r$, $2\omega_0 \pm \omega_r$, *and* $2\omega_0 \pm 2\omega_r$. Similarly, only the component at resonant frequency, ω_r term, is measured using a lock-in-amplifier and it is given by:

$$\Delta z\big|_{\omega_r} = \frac{Q}{2k}\frac{\partial}{\partial z}C(x,y,z)[A - V_c \cos(\phi_p - \phi_c)]K\cos(\omega_r t) \tag{3.25}$$

By adjusting A and ϕ_p until the deflection signal at ω_r is nulled, both amplitude V_c and phase ϕ_c of the signal can be determined.

3.3.6 EFM system theoretical characterization

3.3.6.1 Spatial resolution

In reality, the electrostatic force sensed by an EFM probe is a sum of capacitive couplings induced by different points on the integrated circuit. For example, if an EFM probe is placed above one trace of a bus structure on an integrated circuit, every trace of this bus will have capacitive interaction with the EFM probe, and each trace's interaction is weighted by its separation to the probe, its geometries and the voltage signal it carries. EFM spatial resolution defines how localized the probe-circuit coupling is and how well an EFM probe can perform a signal measurement of the interested conductor with the disturbing interactions from other circuit elements close to the test point. Obviously, the spatial resolution is related to the probe tip to circuit separation and their geometries. In above example, spatial resolution will tell that how close to the bus line the EFM probe have to be so that the other traces' effects on the EFM probe can be neglected.

Theoretical modeling of the probe-circuit interaction has been performed by Said and Bridges [31]. In one case, electrostatic force density was calculated for macroscopic probe and an infinite ground plane at various separations, and spatial resolution was defined as the radius of a circle that marks half of the total electrostatic force on the probe. For a potential difference of 1V, the defined spatial resolutions are 700nm for 100nm separation, and 15μm for 1μm separation respectively. In another case, the force density was modeled for a micromachined cantilever probe over a coplanar waveguide with a 1μm wide center conductor. The force density is graphed, as seen in Figure 3.10 for 1V potential difference and three different distances between probe tip and the conductor surface, 100nm, 200nm, and 500nm. EFM spatial resolution in this configuration is defined as the diameter at which the electrostatic force on the probe drops to 1/*e* of its maximum. It turns out that spatial resolutions are 300nm, 500nm, and 1000nm for the three different separations respectively.

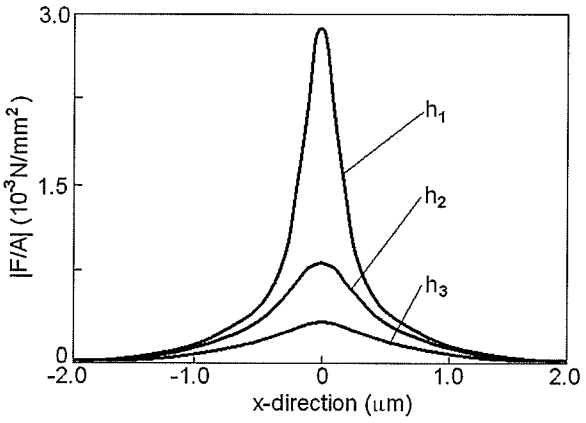

Figure 3.10 Calculated electrostatic force densities for cantilever tip at various heights over a 1μm wide conductor with a 1V potential difference, h_1=100nm, h_2=200nm, and h_3=500nm [33].

Clearly, sub-micron spatial resolution is achievable when the tip-circuit separation is close enough (below 500nm in above case), and the spatial resolution decreases rapidly as the probe to circuit separation increases.

3.3.6.2 Invasiveness

Invasiveness of a probing technique is the degree of undesirable disturbance of the circuit's normal operation. It is in terms of extra capacitance, inductance, or loading resistance introduced by the probe. As EFM probe operates in a non-contact mode, the main source of invasiveness is the capacitive coupling between the conducting probe and the test point. For a micromachined probe over a 3μm wide interconnect line, the coupling capacitance is estimated [32] between 0.23fF to 3fF for probe-to-circuit separation between 1μm to 0.1μm. This coupling capacitance is equivalent to 70kΩ to 5kΩ impedance loads at 10GHz.

3.3.6.3 Voltage Sensitivity

The voltage sensitivity of the EFM probe system is the minimum voltage that can be detected. Overall system noise ultimately limits the performance of this technique.

In [30] and [31], it was identified that the dominant noise source for the EFM technique was the thermal vibration of the cantilever probes. The magnitude of this noise can be represented by the mean-square deflection of the cantilever due to thermal vibration, which is given by:

$$\left\langle z_{th}^2(\omega)\right\rangle = \frac{4kk_bT_aB}{2\pi Q\omega_r}\int_0^\infty \left|G(\omega)\right|^2 d\omega \tag{3.26}$$

where k_b is the Boltzman constant, T_a is the medium temperature, B is the measurement bandwidth, Q is the Q-factor of the cantilever, ω_r is the resonant frequency, and $G(\omega)$ is the cantilever frequency response. Using equation (3.8), the root-mean-square deflection is given as:

$$\sqrt{\left\langle z_{th}^2(\omega)\right\rangle} = \sqrt{\frac{4kk_bT_aB}{2\pi Q\omega_r}}\frac{(Q/k)(\omega_r/\omega)}{\sqrt{1+Q^2(\frac{\omega_r}{\omega}-\frac{\omega}{\omega_r})^2}} \tag{3.27}$$

As $Z(\omega)=F(\omega)G(\omega)$, using equation (3.8) again, this thermal deflection can be re-written in terms of the power spectral density of the electrostatic force F_z, and it is:

$$\sqrt{\left\langle F_z^2(\omega)\right\rangle_{th}} = \sqrt{\frac{4kk_bT_aB}{2\pi Q\omega_r}} \tag{3.28}$$

As expressed in equation (3.4), the power spectral density of the force can also be equated to the voltage that would produce the same force density:

$$\sqrt{\left\langle F_z^2(\omega)\right\rangle} = \frac{1}{2}\frac{\partial}{\partial z}C(x,y,z)\Delta V_{rms}(\omega) \tag{3.29}$$

where $\Delta V_{rms}(\omega)$ is the equivalent RMS potential difference between the probe and device under test. The minimum RMS voltage that can be detected is thus given by:

$$\Delta V_{rms}(\omega) = \frac{2}{\partial C(x,y,z)/\partial z}\sqrt{\frac{4kk_bT_aB}{2\pi Q\omega_r}} \tag{3.30}$$

For the micromachined cantilever used in this research, which has Q=30, k=0.05N/m, and a resonant frequency of f_r=14kHz, being positioned 1 μm above a 3 μm wide inter-connect, this voltage sensitivity is estimated [33] at $1mV/\sqrt{Hz}$.

Chapter 4

EFM and AFM-Based Signal Measurement Techniques and Probing System Architecture

Integrated circuit internal signal measurement is very important to IC failure analysis. This chapter presents a high-speed IC internal signal sampling technique using non-contact electrostatic force microscope and sub-micron contact probing methods using atomic force microscopy. Both EFM and AFM techniques have been integrated in one probing system. The architecture of this testing tool will also be discussed.

4.1 EFM High Speed Pulse Sampling Technique

EFM probing methods for DC potential and basic analog sinusoidal signals were introduced in last chapter. However, a good portion devices of modern microelectronics are digital and square waves are most likely their internal signals. Most real world analog parts also have more complex signal forms inside them than just pure sine or cosine signals. To test them, the more detailed signal characteristics, such as: the state-transition and delay timing information, waveshape, rising/falling times, and relative levels, are often the major interests for their failure analyses. Techniques using EFM to perform such detailed IC internal node waveform measurements have been developed by re-

searchers in University of Manitoba. One of them is the amplitude modulation high-speed EFM sampling technique [42]-[46]. Its study and implementation is the main focus of this research work. This technique utilizes the synchronous high-speed sampling method, an amplitude modulation scheme, and high-precision pulse generator and timing unit in conjunction with EFM operation to perform non-invasive high-speed IC internal probing. Following sections review its detailed theoretical study and its hardware and software system designs.

4.1.1 High speed equivalent-time sampling technique

Sampling technique is always used for waveform measurement. Achieving higher sampling rates requires equivalent-time sampling, the principle of which is illustrated in Figure 4.1. Samplings are collected at a slower rate from different occurrences of a repetitive signal and reassembled according to their sampling phase on an equivalent-time scale.

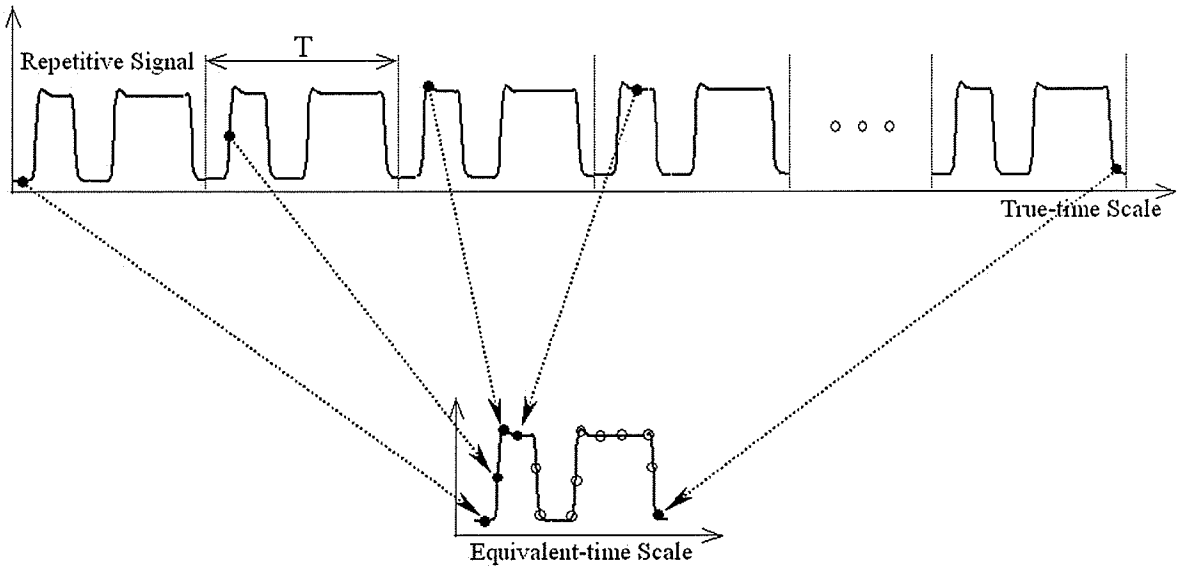

Figure 4.1 high-speed equivalent time scale sampling diagram.

One data point of the extracted waveform may be the average of samplings of a number of repeat cycles at same sampling phase. This averaging improves the measurement signal resolution. The important limitation of this technique is that only repetitive signals

may be measured. This equivalent-time sampling technique requires the sampling signal synchronizes with the circuit signal under test, and the sampling rate equals the signal pattern repeat rate. The period of this rate is also called duty-cycle.

4.1.2 EFM amplitude modulation high-speed sampling technique

An amplitude modulation scheme and equivalent-time scale sampling technique have been combined with EFM operation to accomplish high-speed non-invasive IC internal signal measurements. A block diagram of this measurement method is shown in Figure 4.2. The EFM operating principle has been presented in last chapter. To briefly summarize here, a conducting micromachined cantilever is placed at a small distance above a circuit test point. An electrostatic force is induced on the cantilever due to probe-circuit capacitive coupling and the potential difference between the probe signal $v_p(t)$ and the circuit waveform $v_c(x,y,t)$. The deflection of the cantilever due to this force is sensed by the optical beam bounce system.

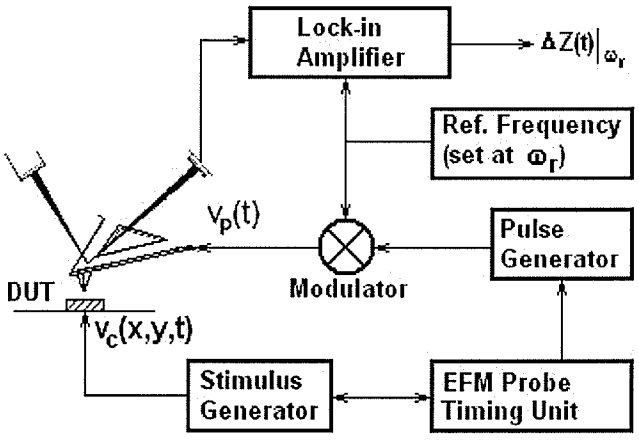

Figure 4.2 Amplitude modulation EFM high-speed sampling technique.

In this amplitude modulation EFM sampling technique, the EFM sampling signal sent to the end of the probe tip is a train of narrow electrical pulses, and they are modulated at the cantilever resonant frequency. Modulating at resonant frequency can enhance the cantilever deflection by a factor of Q, as expressed in equation (3.10). A lock-in amplifier is also set at this frequency so that it can detect the amplitude of cantilever deflection

just at the resonant frequency. The sampling pulse is synchronized with the stimulus signals to the device under test (DUT) through the EFM probe timing unit, as required by the equivalent-time sampling technique. Therefore, the sampling pulse rate matches the duty cycle of the signal to be tested.

The following is the mathematic analysis of this measurement technique based on ideal narrow square sampling pulse and square wave modulation, as illustrated in Figure 4.3.

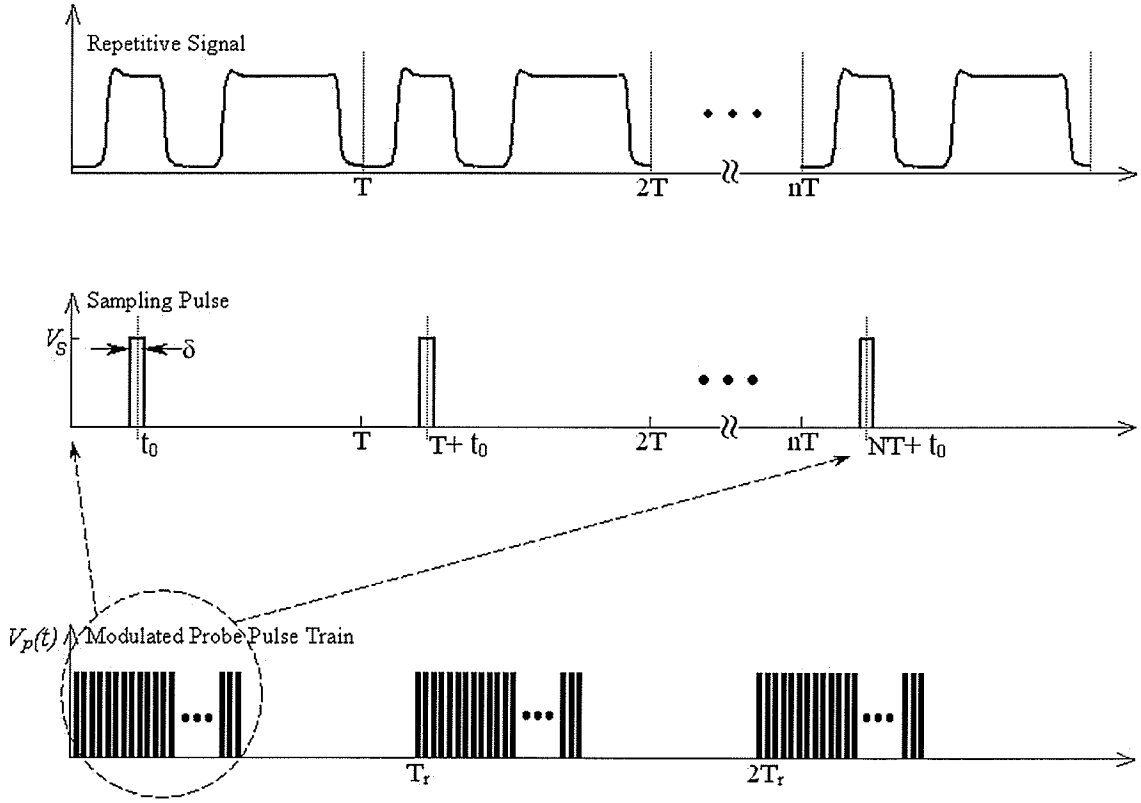

Figure 4.3 EFM amplitude modulated sampling pulse timing diagram.

A simple digital square waveform, shown in Figure 4.3, represents the repetitive signal to be tested. The train of square sampling pulse, as shown in Figure 4.3, can be given as:

$$v_s(t) = \sum_{n=0}^{\infty} V_s G_\delta(t - nT - t_0) \tag{4.1}$$

where V_s is the amplitude of the sampling pulse, T is the repetitive test signal's duty cycle, t_0 is the sampling pulse phase location relative to the repetitive test signal, δ is the sampling pulse width ($\delta << T$), and G_δ is square delta function which can be mathematically expressed as:

$$G_\delta(x) = \begin{cases} 1 & -\frac{\delta}{2} \le x \le \frac{\delta}{2} \\ 0 & x > \frac{\delta}{2}, \quad x < -\frac{\delta}{2} \end{cases} \tag{4.2}$$

The sampling train, also shown in Figure 4.3, is modulated by a square wave at resonant frequency, ω_r. Using Fourier transforms, this square wave can be represented as:

$$V_M(t) = \frac{1}{2} + \frac{2}{\pi} \sum_{m=1,odd}^{\infty} \frac{1}{m} \sin(m\omega_r t) \tag{4.3}$$

Putting them together, the probing signal $V_p(t)$ becomes:

$$V_p(t) = V_s(t) V_M(t) = [\sum_{n=0}^{\infty} V_s G_\delta(t - nT - t_0)][\frac{1}{2} + \frac{2}{\pi} \sum_{m=1,odd}^{\infty} \frac{1}{m} \sin(m\omega_r t)] \tag{4.4}$$

Cantilever deflection induced by the electrostatic force at its resonant frequency, as seen in equation (3.4) and (3.10), is given by:

$$\Delta Z\big|_{\omega=\omega_r} = \frac{Q}{k} F_z(\omega_r) = \frac{Q}{2k} \frac{\partial C(x,y,z)}{\partial z} [v_p(t) - v_c(x,y,t)]^2 \big|_{\omega=\omega_r} \tag{4.5}$$

Since the lock-in amplifier is set to measure the amplitude of this deflection only at the modulating frequency, which is the resonant frequency, using equation (4.3), this deflection term at ω_r is:

$$\Delta Z\big|_{\omega=\omega_r} = \frac{Q}{k} F_z(\omega_r) = \frac{Q}{2k} \frac{\partial C(x,y,z)}{\partial z} [< v_s(t)^2 > -2 < v_s(t) v_c(x,y,t) >][\frac{2}{\pi} \sin(\omega_r t)] \tag{4.6}$$

where $< v_s(t)^2 >$ and $2 < v_s(t) v_c(x,y,t) >$ are the signal averaging terms over the period of duty cycle, T. The $v_c(x,y,t)^2$ term doesn't appear in above equation, as it is a higher frequency term and doesn't have any component at the resonant frequency, cannot be

detected by the lock-in amplifier, and it doesn't have any contribution to equation (4.6). The DC and higher order resonant ($m\omega_r$, m=3, 5, 7...) terms of the $2 < v_s(t)v_c(x,y,t) >$ production are not detected by the lock-in amplifier either, and they are not included in above equation.

Using square sampling pulse train expression (4.1), we get:

$$< v_s(t)^2 >= \frac{1}{T}\int_0^T \sum_{n_1=0}^{\infty} V_s G_\delta(t - n_1 T - t_0) \sum_{n_2=0}^{\infty} V_s G_\delta(t - n_2 T - t_0) dt = \frac{\delta}{T} V_s^{\,2} \tag{4.7}$$

$$\begin{aligned} < v_s(t)v_c(x,y,t) >&= \frac{1}{T}\int_0^T \sum_{n=0}^{\infty} V_s G_\delta(t - n_1 T - t_0) v_c(x,y,t) dt \\ &= \frac{1}{T} V_s \int_{t_0-\frac{\delta}{2}}^{t_0+\frac{\delta}{2}} v_c(x,y,t) dt \end{aligned} \tag{4.8}$$

The first average is a constant term to all pulse phase location. The second term is proportional to the desired waveform amplitude average over the sampling pulse window δ, at relative phase location t_0. For very narrow sampling pulse approximation, equation (4.6) becomes:

$$\Delta Z\big|_{\omega=\omega_r} = \frac{Q}{k} F_z(\omega_r) \approx \frac{2Q}{k\pi} \frac{\partial C(x,y,z)}{\partial z} V_s^{\,2} \frac{\delta}{T} [\frac{1}{2} - \frac{1}{V_s} v_c(x,y,t_0)] \sin(\omega_r t) \tag{4.9}$$

This equation defines that the deflection amplitude measured by the lock-in amplifier is proportional to the circuit waveform's amplitude at the sampling pulse position.

Equation (4.9) is represents only one point of the waveform at time t_0. By shifting the sampling pulse's relation phase to the repetitive waveform, the measured waveform is constructed from a series of points corresponding to different pulse phases, as shown in Figure 4.4.

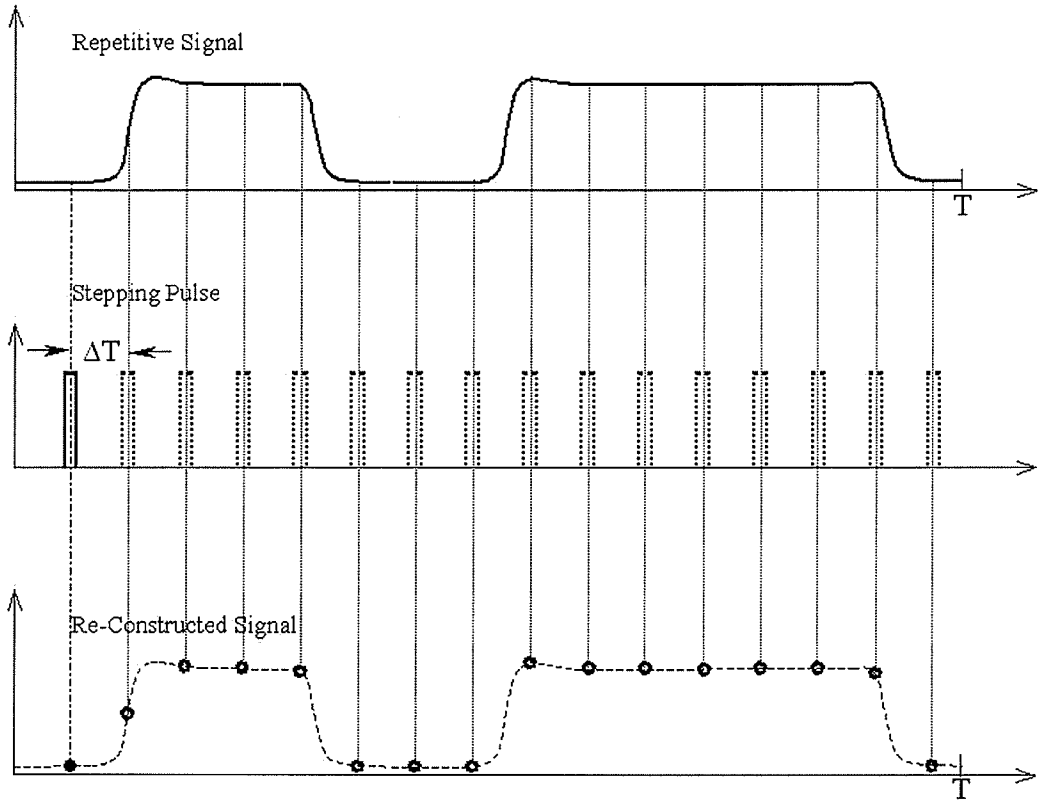

Figure 4.4 Waveform extracting by EFM sampling pulse shifting.

Some properties of this measurement technique are summarized here as results from above theoretical analysis.

Measurement accuracy and bandwidth are determined by sampling pulse width. According to equation (4.8), shrinking the sampling pulse width δ increases the accuracy and bandwidth of the measurement. However, as seen in equation (4.9), it also reduces the detectable amplitude of the deflection, and in turn affects the signal-to-noise ratio. Applying convolution and de-convolution techniques to equation (4.8), bandwidth of the sampling system can be calculated out. For the rectangular sampling pulse, the 3dB bandwidth of the system is:

$$f_{3dB} \approx \frac{0.604}{\delta} \tag{4.10}$$

while for a Gaussian shape sampling pulse, the 3dB bandwidth [34] is:

$$f_{3dB} \approx \frac{0.44}{FWHM} \tag{4.11}$$

where *FWHM* is the full width of a Gaussian shaped sampling pulse at its half amplitude. As seen later, electrical pulses of a 100ps width can be generated, and it corresponds a 3dB measurement bandwidth of 3.1GHz.

The propagation delay between two test points is independent of the pulse width and shape as long as pulse width is much smaller than the waveform duty cycle. A simple delay measurement may be obtained by taking some amplitude features, such as rising and falling edges, that can be traced between the two waveforms; the measurement accuracy is then determined by the phase-shifting accuracy of the sampling pulse. However, for fast rising/falling edges, it is required that the sampling pulse width is sufficiently short to resolve them. This delay measurement technique will be demonstrated in next chapter.

To get more detailed information of the waveform, the sampling pulse needs to be stepped at very fine time intervals. In fact, the timing unit we used in this research can shift sampling pulses as fine as 1 picosecond a step. On the other hand, as the time for the EFM probing system to acquire one data is limited to a certain minimal time by overall system signal-to-noise ratio and the response time of lock-in-amplifier, finer stepping may result longer measurement time for the whole waveform.

The duty cycle T is another parameter that works again the system signal-to-noise ratio, as expressed in equation (4.9). Thus it is generally desirable to edit the test stimulus patterns so that to reduce the length of the digital vector to be measured. The absolutely limitation of this modulation scheme is set by the period of cantilever mechanical resonance. For a 10KHz resonant frequency, it is 0.1ms, and it is equivalent to 100 thousand digital bits for a 1GHz microprocessor.

4.1.3 Narrow pulse generation

A pulse generator, as seen in Figure 4.2, is used to produce the high-speed sampling pulse train $v_s(t)$ in amplitude modulation. The system performance, such as bandwidth

and accuracy, largely depends on the properties of sampling pulse. The ideal pulse would be one with high amplitude and pulse width could be controlled down to very narrow duration. This section reviewed a few pulse generators and techniques used in this research work.

4.1.3.1 Digital pattern generator

Commercial high-end digital pattern generators from Aglient or Tektronix are usually capable of producing bit rates up to several Gbit/s, and they can also generate electrical pulses with widths as small as few hundreds of picosecond. A Tektronix HFS9000 digital pattern generator, shown in Figure 4.5, is used in this research work as timing unit, pulse generator, as well as digital stimulus signal sources. It is able to produce 800ps pulses with rising and falling times of less than 200ps. Its timing resolution is at a remarkable value of 1ps. As mentioned in last section, we can shift the sampling pulses as fine as 1ps a step to perform a very detailed measurement of the interested rising or falling edges of the waveforms, and perform propagation delay calculations.

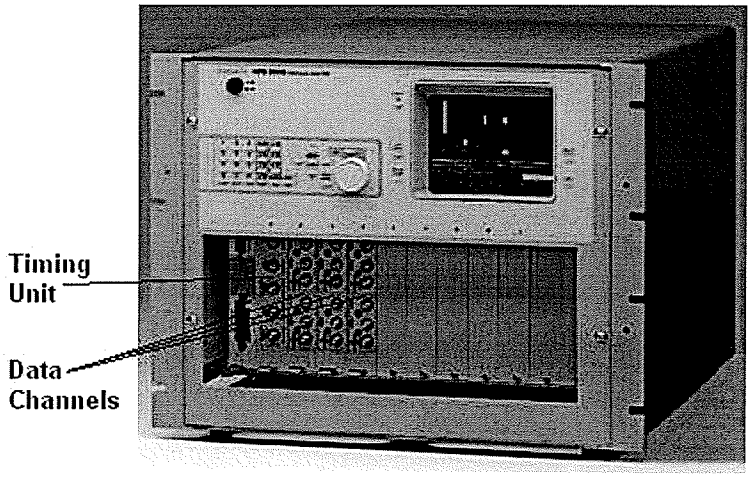

Figure 4.5 Photo of the Tektronix HFS9000 digital data generator.

4.1.3.2 Transmission line filter

Transmission line filter can be used as simple but effective pulse generator [35]. Passive high-pass filters can be made of 50Ω transmission lines. Figure 4.6 shows one design of such filters. It is constructed by placing two short-circuited 50Ω coplanar stubs at the

same location of another 50Ω coplanar line to form a cross-shaped circuit. The whole filter can be fabricated as a piece of PCB or it can simply be built by high quality co-axial 50Ω cables. The lengths of the two stubs are optimized so that the output of this filter is the derivative of the input signal. Then, this high-pass filter will translate fast rising or falling edges of input signal to positive or negative pulses at output.

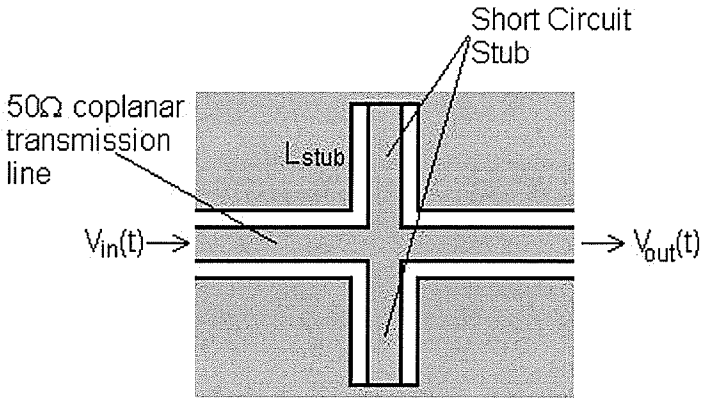

Figure 4.6 50Ω transmission line pulse generator.

Figure 4.7 illustrates measured waveforms of narrow pulses generated by the high-pass transmission line filter. As seen in Figure 4.7, the input signal is a square wave with 200ps rising and falling times. After the filter, there are two narrow pulses on output signal; one positive and one negative correspond to the input rising and falling edges respectively. The widths of them are determined by the rising and falling times, and their FWHM is measured at 400ps. A RF-MUX is also used to gate out the un-desired negative pulse. Gating signal and final pulse are shown in Figure 4.7 too.

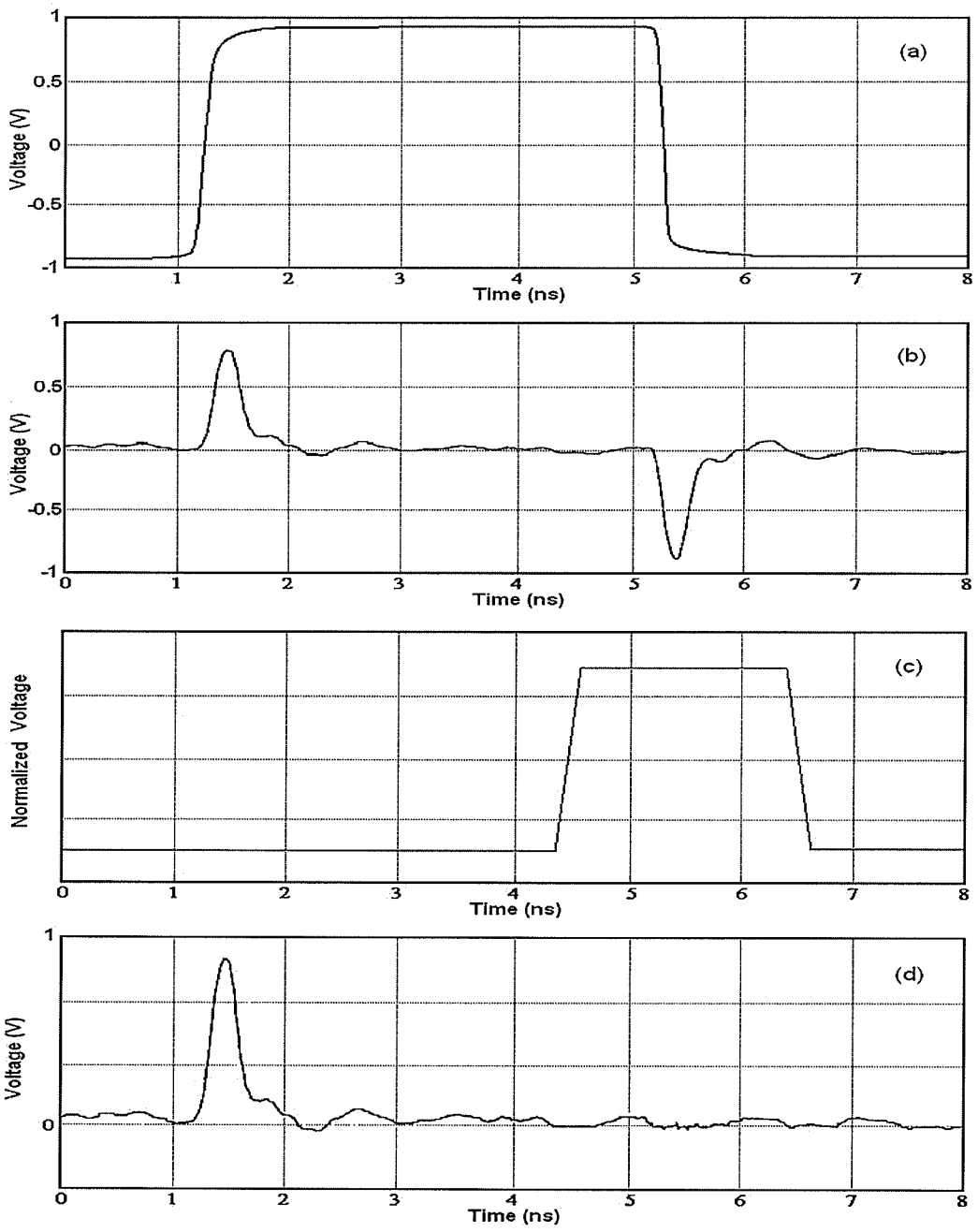

Figure 4.7 Measured signals of a 50Ω transmission line pulse generator.

4.1.3.3 Step recovery diode

The high-pass transmission line filter is an effective device to generate narrow pulses, however it needs the input signal having very fast rising or falling times in the first place.

A step recovery diode (SRD) is able to produce such fast edges. A SRD is a non-linear charge storage device. The capacitance of the SRD is large under forward bias and is small under reverse bias. As it is driven by a input sine wave, it accumulates charges when the sine signal is at forward bias. Due to the small reverse bias capacitance, the rate of SRD's reverse discharging is quite high, thereby forming a very fast step. For example, a commercial SRD [36] used in this research can generate rising or falling edges as fast as 100ps. Combining the SRD and the high-pass transmission line filter technique, 100-150ps FWHM wide pulses can be produced.

4.2 Probe System Architecture

4.2.1 Probe System Structures

EFM operation is very sensitive to mechanical vibration. The probe system should be designed with high rigidity and usually operates on a vibration-isolation table so that to reduce noise due to inherent mechanical vibration. Two version of EFM probing systems were designed during the course of this research.

The first design was a prove-of-concept laboratory unit, as shown in Figure 4.8. There are two levels of this stage. The lower platform forms the based of the unit, and the sampling stage and positioning system are located on this platform. The upper platform supports the Laser deflection detection system, and has the cantilever holder screwed securely underneath the center of this plate.

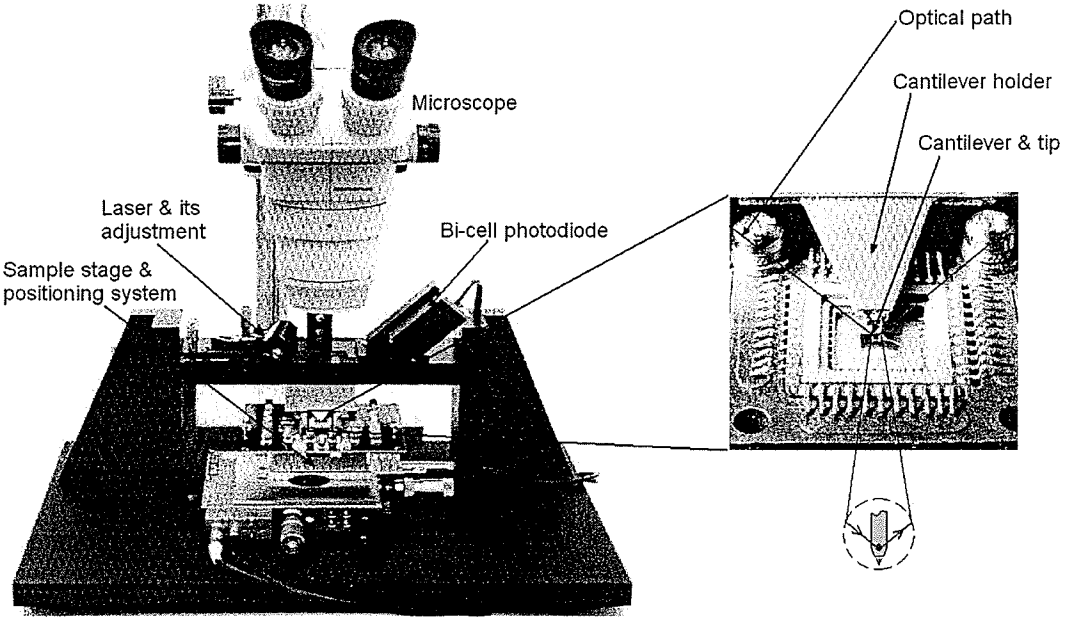

Figure 4.8 Photograph of a laboratory EFM system.

The cantilever, as seen in the enlarged picture in Figure 4.8, is mounted onto the end of a 50Ω coplanar transmission line of the probe holder so that the high frequency sampling pulse can transmit to the end of it without degradation. The impinging Laser beam from one side of the probe is focused on the end of the cantilever and reflected to the bi-cell photodiode located on the other side. Alignment and adjustment of the Laser beam deflection detection system can be done manually using micrometer screws. Test sample's coarse movements are performed by the computer-controlled XYZ stage. A piezo tube scanner (Its operating principle is discussed in last chapter) is mounted on top of the XYZ stage to hold the test samples. High-resolution AFM imaging is performed by this piezo tube scanner.

In order to apply EFM probing technique to more practical applications, another probing system has been designed to retrofit a probe station. A probe station is a very common tool in IC manufacturers' failure analysis lab. It provides functionally flexible and mechanically stable platform for mounting probes and probe cards. As shown in Figure 4.9, the EFM probe head has be designed into a very compact size, yet it includes all functional blocks of an EFM system. This probe system utilizes the existing probe station microscope and sample positioning systems. It is integrated with the probe cantilever holder, high-resolution scanner, Laser deflection detection system and some other

high-resolution scanner, Laser deflection detection system and some other functional blocks into a probe head. Details of the probe head will be reviewed in the following sections.

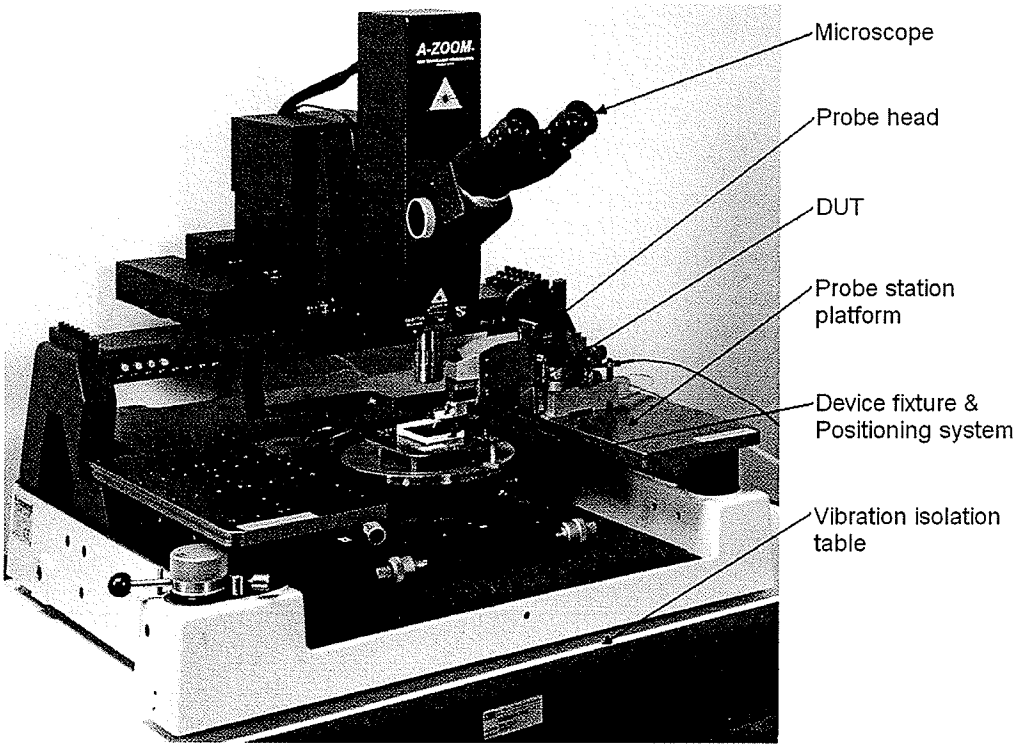

Figure 4.9 Photograph of and EFM probing system mounted on a typical probe station [37].

4.2.2 Probe Head and Probe Tip Assembly

An enlarged photograph of the probe head is shown in Figure 4.10. From the bottom of the probe head, there is a vacuum device to hold it on the probe station platen. This is also the common practice for a mechanical needle probe head. As shown in Figure 4.10, the manual XY-axis adjustments are used for coarse movement. The manual Z-axis slide adjustment is to raise and lower the probe head toward the test sample surface upon initial setup. The Z-axis linear actuator is for computer-controlled coarse adjustment. A Piezo actuator is used for fine movements in X, Y, and Z axes to perform precise probing positioning and high-resolution imaging. The piezo actuator is integrated with the probe head instead of test sample stage for practical reasons. For instances, the devices under

test may be too heavy to move linearly by piezo actuator, or they may tie to the stimulus fixture and cannot be moved. The most important reason is that failure analysis on some integrated circuits may involve several probes on a same device simultaneously, and this requires that any probe movement must be independent of sample movements. Figure 4.10 also shows a high frequency coax cable on the side of the probe head, which is used to connect the pulse generator of the system to the tip assembly. It is also used to connect contact probe to measurement equipment in contact probing configuration, which will be discussed later.

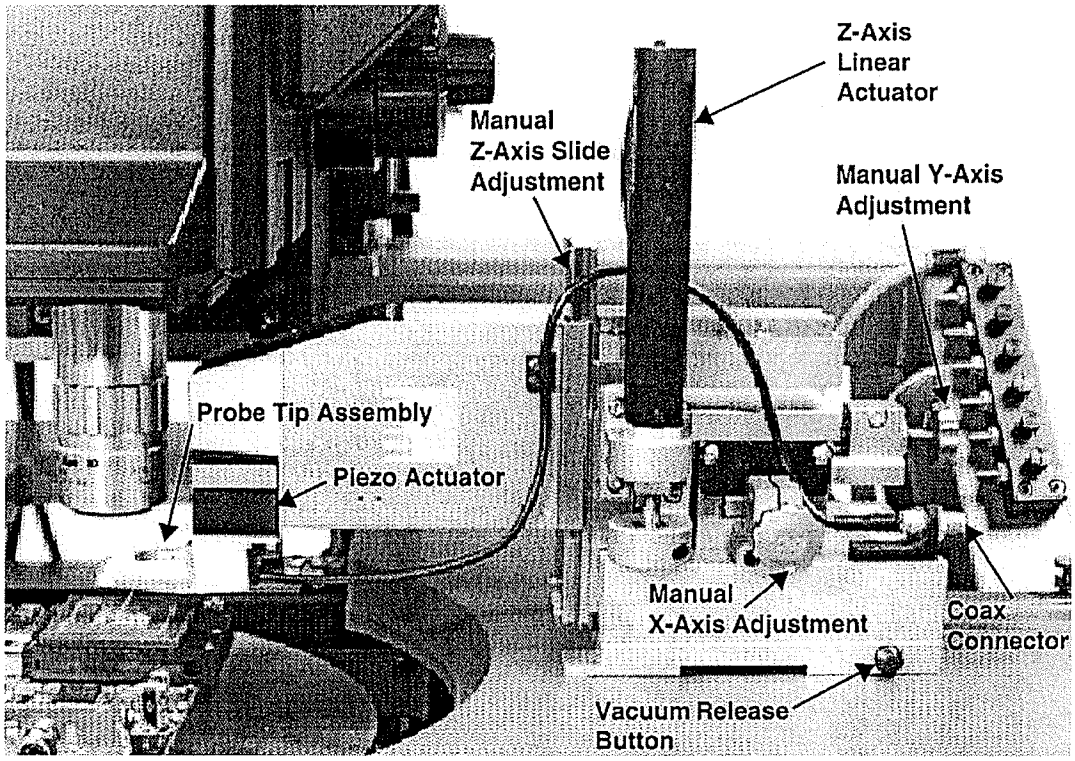

Figure 4.10 A detail photograph of the EFM probe head.

Laser beam deflection detection system is housed inside the probe arm. Both Laser source and bi-cell photodiode are driven by micro-motors for computer-controlled automation. In order to make this compact size, the optical path of the deflection detection system is designed differently from the laboratory system. Figure 4.11 illustrates the optical path of the probe system. A 50% beam splitter is used to integrated impinging and reflected beams into one path. Unlike the laboratory system, the Laser beam is at per-

pendicular angle and straight onto the cantilever surface in this configuration. This arrangement dramatically reduces the size of Laser beam deflection detection system, and also utilizes the full cantilever deflection range. Couplings between adjustment axes of the Laser source and photodiode are kept at minimum in this configuration, and it makes the Laser beam deflection detection system calibration and automation simple and easy.

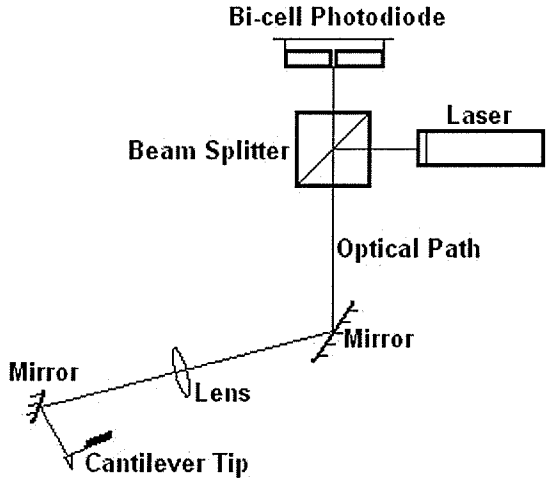

Figure 4.11 Optical path of the deflection detection system.

The photodiode's currents are translated to voltages by its receiving and amplifying circuit in order to facility the digitalizing process of the data acquisition module. The circuit, as shown in Figure 4.12, converts the photodiode currents of two cells (A and B cells) to voltages and outputs the sum and the difference signals of them. They are expressed as:

$$V(A+B) = \frac{R_2}{R_1} R_0 (i_A + i_B) \tag{4.12}$$

$$V(A-B) = \frac{R_2}{R_1} R_0 (i_A - i_B) \tag{4.13}$$

where i_A and i_B are photocurrents from cell A and B respectively, and $\frac{R_2}{R_1} R_0$ term represents the gain of these two stage operational amplifiers. C_0 and R_0 form a low-pass flitter to reduce the system high frequency noise above the cantilever resonance.

The sum signal *V(A+B)* is proportional to the total Laser power been reflected by the cantilever, which is used by the control system in the Laser auto-focus and deflection detection system automatic setup procedures. The difference *V(A-B)* is proportional to the cantilever deflection, which is the most important signal for EFM probing operation, and used for EFM high-speed waveform sampling.

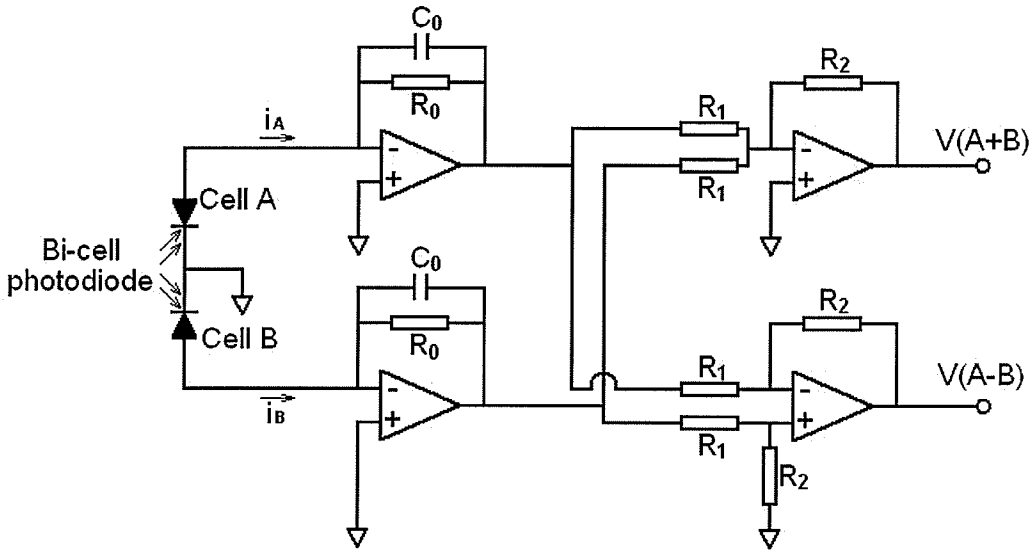

Figure 4.12 Photodiode current-to-voltage and amplifier circuit.

The probe cantilever tip is integrated in an interchangeable unit, as seen in Figure 4.13, which is call probe tip assembly. It can be replaced when the tip wears out or a different type of tip is used. In the front of this assembly is a mirror which reflects the Laser beam and is part of the optical path, as seen in Figure 4.11. The cantilever tip is mounted at end of a ceramic circuit board. For an EFM non-contact probe tip assembly, on the back of the board is a 50Ω coplanar transmission line which connect the probe tip to the high frequency cable seen in Figure 4.13 through a high frequency connector in the mating interface, and high-speed sampling signal is carried in this conducting path. For a contact

probe assembly, there will be different circuitries on the back of the ceramic board to perform other probing functions, which we will review in later sections. The probe assembly is inserted into the probe head. A registration pin is used to ensure that tip positions are consistent within certain mechanical error in order to serve Laser auto-calibration procedure.

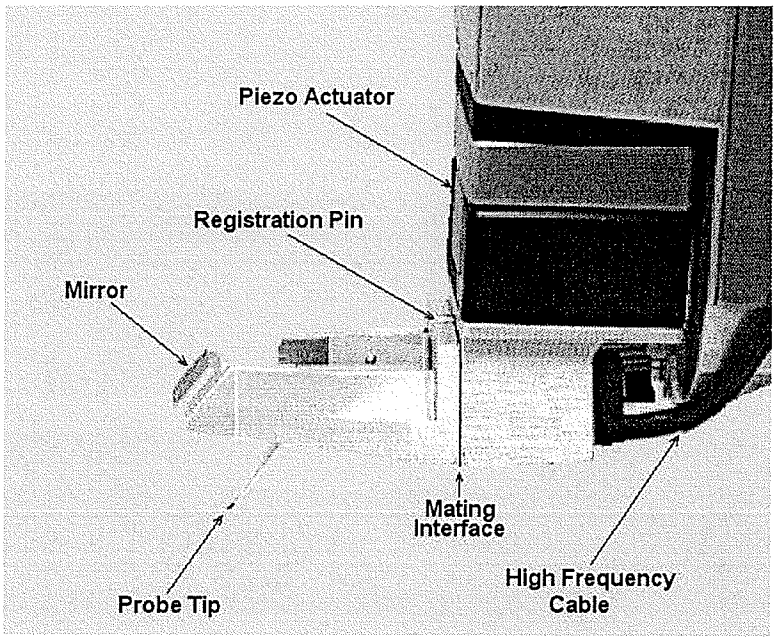

Figure 4.13 A close view of probe tip assembly [37].

4.2.3 Control system and application software

A block diagram of the entire EFM probe system is shown in Figure 4.14. Timing unit controls the sampling pulse shifting and may send out or receive trigger signals for synchronization with a device under test. Pulse generator and modulator produce the modulated sampling pulse train for EFM probing. Probe control unit is a digital-to-analog converter (DAC) board which generates the controlling signals for all micro-motors of deflection detection system, linear actuator and piezo actuator. Data acquisition is performed by an analog-to-digital converter (ADC) board which works in conjunction with lock-in amplifier to collect and digitalize the photodiode signals. Spectrum analyzer is used to monitor the probe cantilever frequency response and to locate the resonant fre-

quency of it. Finally, the probe head is connected to the control blocks via a high-speed coax cable for the sampling pulse and a cable harness for all rest signals. The host computer communicates with the ADC and DAC board via a PCI bus and other instruments via a GPIB bus. The probing system application software runs in the host computer.

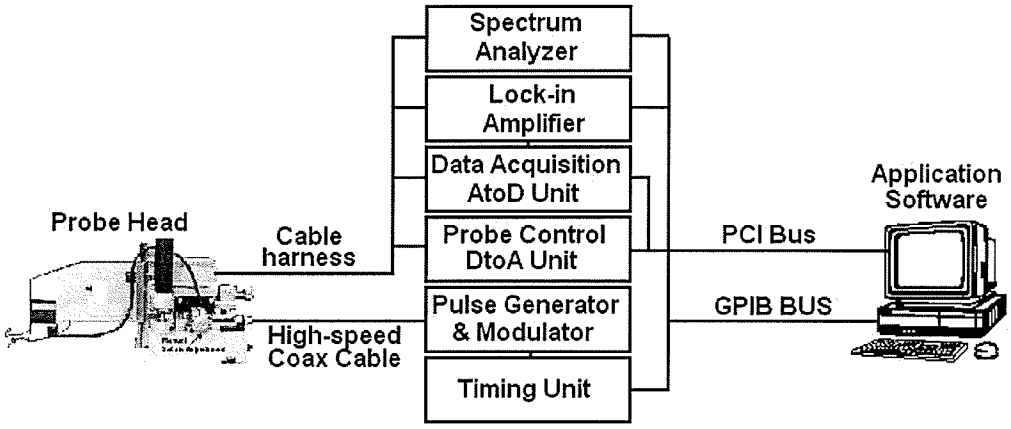

Figure 4.14 System block diagram of an EFM probing system.

Besides coarse initial setup and few manual adjustments, all other functions are computer-controlled through software. An interface of the software is shown in Figure 4.15.

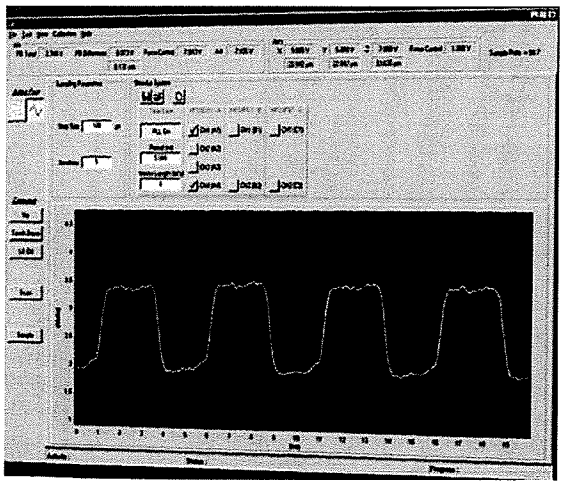

Figure 4.15 Picture of the application software interface of the probing system.

Major computer-controlled functions of the probe system are summarized as follows:

- **Cantilever searching and Laser auto-focusing.** As mechanically designed, every time a tip assembly is inserted into the probe head the cantilever tip of this assembly is located in the space within certain error. This mechanical property enables the searching algorithm, with the help from V(A+B) signal from photo-diode circuit, being implemented in software.

- **Laser deflection detection system auto-calibration.** This is mainly the computer-controlled photodiode movement after Laser is focused in previous procedure. The photodiode is moved so that the initial V(A-B) signal is close to zero to balance the deflection detection range.

- **Initial tip touchdown to find the test sample surface.** EFM cantilevers are very fragile structures. Its initial touchdown must be computer-controlled. To perform this procedure, computer-controlled Z-axis linear actuator lowers the probe arm, while V(A-B) signal of deflection detection system is monitored. Once the signal jumps and passes certain pre-set threshold, the host computer realizes that the test sample surface is found.

- **High-resolution surface imaging.** The procedure will be discussed in details in the contact probing section later.

- **Probe positioning and EFM signal sampling.** The probe is driven by the piezo actuator after a surface image is taken. Clicking on the image results the probe moving to the corresponding point on the test sample. The controls of the EFM signal sampling are reviewed in the following paragraphs.

The application software controls the EFM signal sampling procedure through a set of parameters.

- **Tip-to-surface separation.** Tip-to-surface separation can be controlled precisely through peizo Z-axis actuator. Theoretically, it should be set as small as possible to increase the electrostatic force; practically, taking into account the vibration noise level for a normal test environment, it is optimized at around 300nm.

- **The modulation frequency.** Most of the time, it is set to the resonant frequency of the cantilever.

- **The sampling pulse width and amplitude.** Although the sampling technique prefers larger pulse amplitude, the sampling pulse amplitude is limited by the hardware of pulse generator and it is pre-set. As discussed in the theoretical analysis, narrower pulse width increases the measurement accuracy and bandwidth, yet larger pulse width enhances the signal-to-noise ratio.

- **Single point sampling time.** It is the duration that the sampling pulse stays at one phase position. The duration is actually divided into two time slots. The first duration is the system stabilization time after the sampling pulse shifting from one phase to another, and it is set at 100ms based on the overall system response. The second duration is data acquisition time by ADC board, and this time is usually around few hundred milliseconds. The ADC board samples at 200kHz, and all sampled data averages into one data point. This averaging effectively reduces higher-frequency system noise.

- **Pulse stepping interval.** It is the time step to construct the whole measured waveform. It can be as fine as 1ps, since the timing unit has a resolution of 1ps. However, finer step increases the measurement time. A "zoom-in" sampling feature is also implemented in the software, which allows a coarse sampling at a larger stepping interval, and fine sampling to an interesting portion (zoom-in) of the waveform. This feature is particularly useful when measuring a rising/falling edges or delays.

- **Waveform loops.** This is to set how many times a waveform is sampled, and all data can be averaged into one final waveform. The feature reduces the low frequency system drifting effect.

4.3 AFM-based Sub-micron Contact Probing Technique

Techniques for waveform measurement may be broadly divided into real-time measurements and equivalent-time sampling. We have reviewed EFM probing system for equivalent-time waveform sampling, and the system has also been applied on real-time measurements. Real-time measurement has the ability to capture single-shot or asynchronous events, which cannot be tested by sampling techniques because those signals are not repetitive. Real-time signal probing usually requires contact access to test point. This section presents the AFM-based sub-micron contact probing technique.

4.3.1 AFM imaging

The size of the integrated circuit elements comprising present day ICs can be less then 0.25μm and cannot be seen clearly using conventional probe station microscope. Under optical microscope, even at substantial magnification, two 0.25μm devices, positioned 0.25μm apart, cannot be resolved. In addition, as device geometry shrink to sub-micron, accurately positioning the traditional wire probe tip to make a reliable electrical contact is getting harder and harder if it is not impossible. Fortunately, AFM is able to perform surface imaging at nanometer resolution which is much higher than optical resolution. We demonstrate that sub-micron probing methods by combining AFM and contact probing techniques.

The AFM-based contact probing system utilizes the same probe head. However, the probe tip assemblies are different from non-contact EFM measurement, as contact AFM probes include probing circuitries for contact measurements. The control system is simpler than EFM probing setup. As seen in Figure 4.16, the contact probing system has the host computer which runs the same application software and has the same analog-to-digital data acquisition and digital-to-analog control boards inside it. All other elements shown in Figure 4.14 for EFM probing are not needed in this AFM-based contact probe configuration.

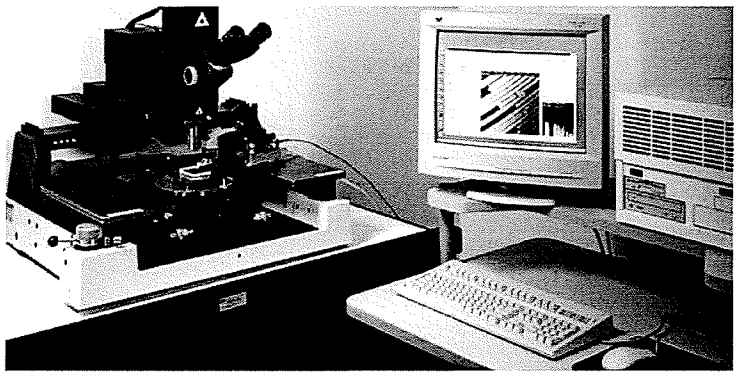

Figure 4.16 An AFM-based contact probe setup [37].

An open loop scan method is adopted to simplify the probe head and control system hardware design requirements. In the open loop scan, the piezo actuator scans a sample surface without feedback signal from deflection detection system. It could be understood as "constant-height scanning" as opposing to "constant-deflection scanning". The topographic information is then given by the cantilever deflection signal.

A question arises for this method, and that is the test sample may be mounted at an angle, as seen in Figure 4.17 (b), to the pure constant-height (where Z-axis peizo actuator is kept at constant value) scanning plane, then it may cause the deflection detection system to saturate at one end of the scan due to limited deflection detecting range of about ±2μm of the deflection detection system. To solve this problem, a plane correction algorithm is implemented in the scan control software. As shown in Figure 4.17 (a), before any largest scan (which is 40μm×40μm as defined by the peizo actuator used), the tip is controlled by the peizo actuator and deflection detection system to make surface-finding touchdowns at four corner points of the scan area, (0,0), (40,0), (0,40) and (40,40), and the corresponding Z-axis piezo positions are recorded.

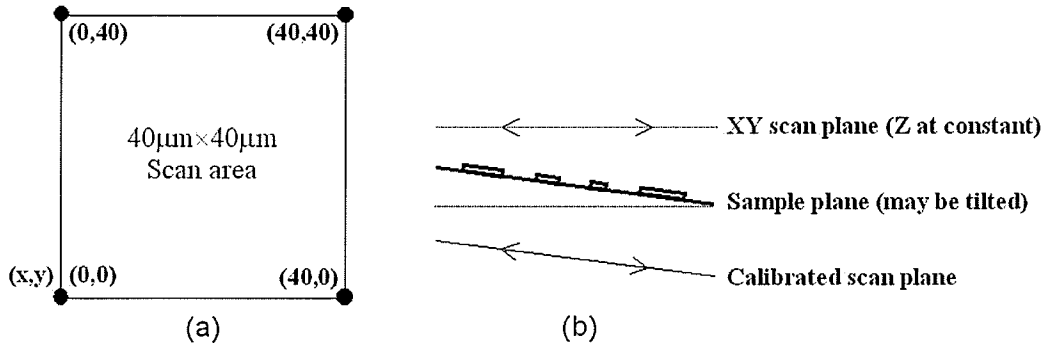

Figure 4.17 Plane correction algorithm of the AFM open loop scan.

A general plane in the space can be represented by a function as:

$$Z = aX + bY + c \tag{4.14}$$

where *a, b* and *c* are there coefficients of the equation, and they can be determined by the measured touchdown data of the three corner points. The forth point data is only used to confirm the calculated results. Therefore, the peizo actuator can scan at a plane to following the sampling tilt by applying a calibration voltage to Z-axis piezo actuator during scanning. The calibration Z-axis piezo voltage for plane correction is given by:

$$V_{peizo}(z) = aV_{peizo}(x) + bV_{peizo}(y) + c / D_{33} \tag{4.15}$$

where, a, b, and c are calculated coefficients, and D33 is the peizo effect coefficient (for the piezo actuator, it is 40μm/150V for all 3 axes).

The system imaging resolution is determined by the piezo actuator resolution and most importantly by the probe tip sharpness. The piezo actuator used in this work has movement ranges of 40μm by 150V for all 3 axes. The control system used on this work is a 16-bit analog-to-digital board. This translates to a 0.61nm minimal piezo step. AFM probes are made by micromachined technology. It is capable of fabricating very sharp cantilever tips. As a tip's SEM image is shown in Figure 4.18, the AFM contact probe tip can be as sharp as 20nm.

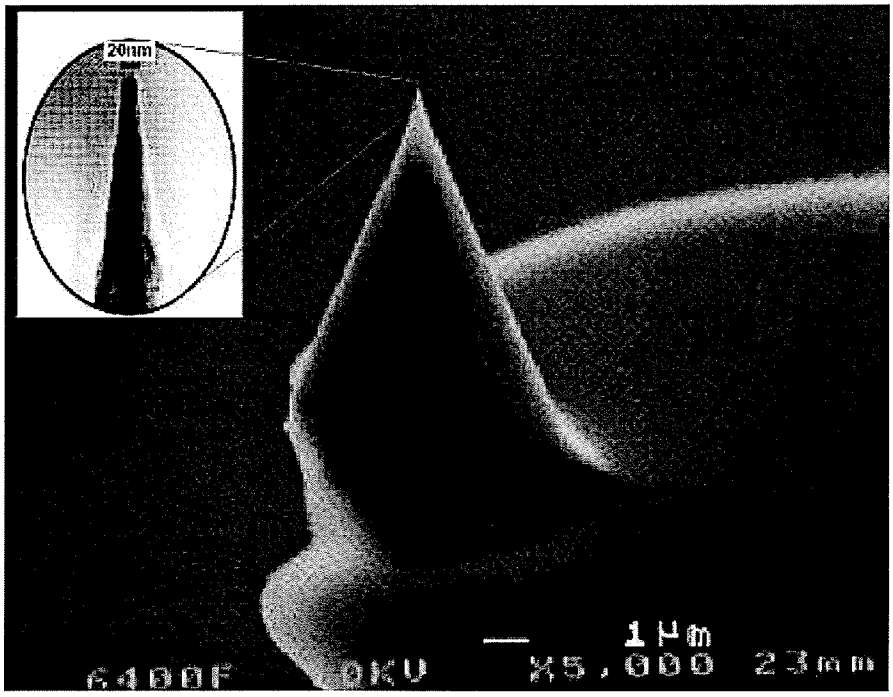

Figure 4.18 SEM image of an AFM probing tip.

The scanned AFM image is displayed on a 256x256 pixel area by the application software. A zoom-in scan can be taken by just dragging a smaller rectangular on the existing image and ask the system to scan again. This zoom-in process is only limited by the hardware limitation as mentioned before. Figure 4.19 shows two images of a serpentine test structure taken by this AFM-based contact probing system. Figure 4.19 (a) is a 40μm×40μm image indicating that at this resolution, one can clearly see sub-micron surface details. To obtain more details of the test structure, a zoom-in scan was taken over 5.8μm×5.8μm area on the same structure and image is displayed in Figure 4.19 (b). The imaging capability of the AFM probe far exceeds that obtainable from an optical microscope. Sub-micron circuit elements are clearly resolvable in the images. Probing procedure is realized by clicking on a interconnect line in the image and the probe positioning is controlled by the piezo actuator. The touchdown force is also monitored by the deflection detection system to maintain a stable contact between the tip and the test trace.

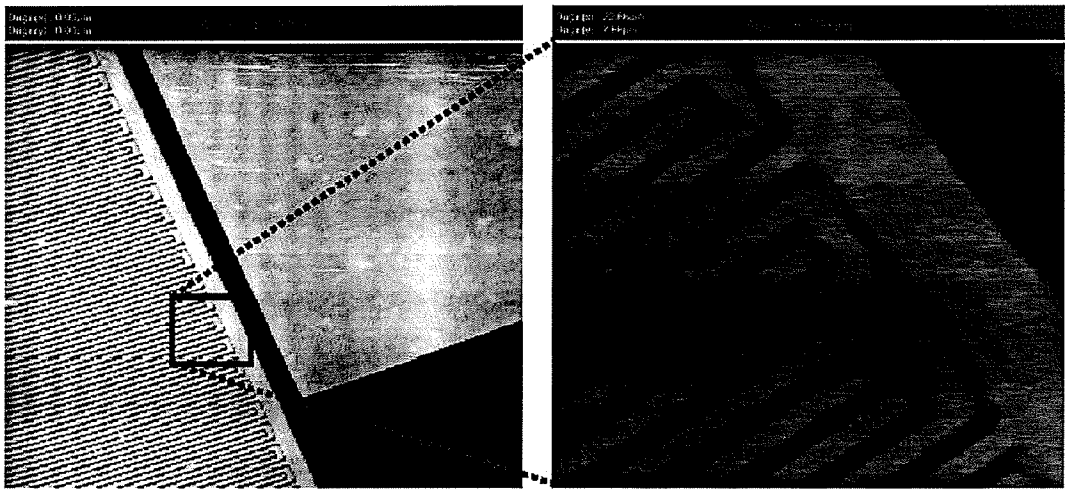

Figure 4.19 (a) AFM 40μmx40μm image of a 0.25μm serpentine test structure on a chip, and (b) AFM zoom-in scanned image of the 5.8μmx5.8μm area indicated by the square on the 40μmx40μm image.

4.3.2 Electrical Analyses of AFM-based Contact Probes

As reviewed in chapter 2, there are several kinds of contact probes. I was involved in integrating two of them with this AFM-based probing system, the passive resistor-divider and active contact probing techniques.

Contact probe circuitries are preferred to be as close to the probing point as possible. In the AFM-based contact probing system, they are built on the circuit boards that the AFM probe tips are mounted on, as shown in Figure 4.20. The following sections analyze their electrical capabilities.

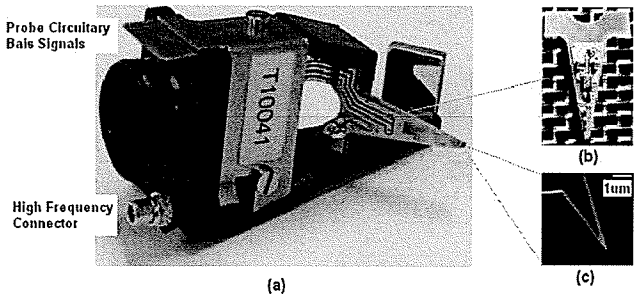

Figure 4.20 Photograph of a contact tip assembly.

4.3.2.1 Passive Contact Probe

A passive contact probe utilizes the resistor-divider technique. It can be built by inserting a resistor in the middle conductor of a 50Ω transmission line, as shown in Figure 4.21 (b). The equivalent circuit of this passive contact probe is given in Figure 4.21 (c).

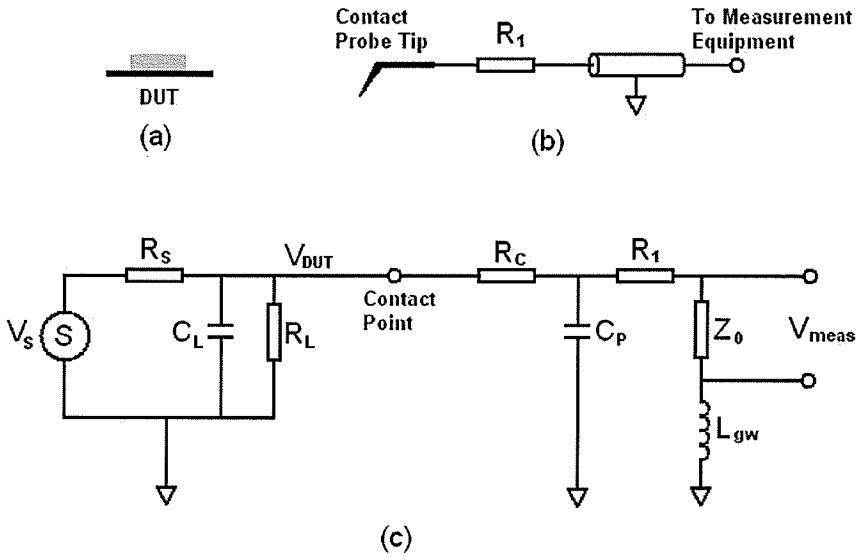

Figure 4.21 Passive contact probe diagram. (a) device under test, (b) the probe implementation, and (c) equivalent circuit.

Where R_S, C_L, and R_L are test circuit's internal loads, V_{DUT} is the signal to be measured, R_c is the contact resistance between the probe tip and test point, C_p is the parasitic capacitance of the probe, R_1 is the signal-dividing resistor, Z_0 is the measurement equipment impedance, L_{gw} is the ground wire parasitic inductance, and V_{meas} is the measured voltage.

Typical values of these parasitic parameters for the AFM-based contact probe system are: C_p=0.1pF estimated by using same method as in [32], and L_{gw}=50nH estimated using a 5cm long ground wire and 1nH/mm [38]. Z_0 is always 50Ω for impedance match at high frequency measurement. R_1 should be 450Ω for a 10-to-1 divided ratio, and 4950Ω for a 100-to-1 ratio.

According to the equivalent circuit, for typical bandwidth below 1GHz, the measured voltage can be given as:

$$V_{Meas.} \approx V_{DUT}\left(\frac{Z_0}{R_c + R_1 + Z_0 + j\omega L_{gw}}\right) \quad for \quad \frac{1}{j\omega C_p} >> R_1 + Z_0 + j\omega L_{gw} \qquad (4.16)$$

where ω is the angular frequency, and $\omega = 2\pi f$.

Evaluating the above equation and equivalent circuit, there are three cut-off frequencies of the system, f_{c1}, f_{c2}, and f_{c3}, and they can be expressed and estimated as:

$$f_{C1} = \frac{1}{2\pi C_p R_c} \approx \begin{cases} 3.5GHz & for \quad R_c = 50\Omega \\ 0.3GHz & for \quad R_c = 5k\Omega \end{cases} \qquad (4.17)$$

$$f_{C2} = \frac{1}{2\pi\sqrt{C_p L_{gw}}} \approx 2.0GHz \qquad (4.18)$$

$$f_{C3} = \frac{R_1 + Z_0}{2\pi L_{gw}} \approx \begin{cases} 1.6GHz & for \quad R_1 = 450\Omega \\ 16GHz & for \quad R_1 = 4950\Omega \end{cases} \qquad (4.19)$$

According to Equation (4.17), maintaining a smaller contact resistance is very important to the measurement bandwidth. The electrical load seen by the DUT from the probe system is mainly the R_1 within the measurement bandwidth. It is the extra load to the DUT; in another words, it is the invasiveness to the DUT. It is preferred to be large.

At DC condition, equation (4.16) becomes:

$$V_{Meas.}\big|_{DC} = V_{DUT}\frac{Z_0}{R_1 + Z_0}\left(1 - \frac{R_c}{R_c + R_1 + Z_0}\right) \qquad (4.20)$$

where $\frac{Z_0}{R_1 + Z_0}$ term is the divided ratio of the probe system, and $\frac{R_c}{R_c + R_1 + Z_0}$ represents an measurement error term, which is related to the contact resistance. At perfect contact condition, it is zero. Normally, the contact resistance can be as low as few Ohm.

However, as the contact is provided the probe conducting coating and it does wear out after certain number of tests. In that situation, the tip assembly has to be replaced.

4.3.2.2 Active Contact Probe

An active contact probe system has an active circuit integrated acting as a buffer in the probe tip assembly. As seen in Figure 4.22 (b), an unprotected field effect transistor (FET) is used as the front amplifier and signal buffer for active contact probe. The equivalent circuit of the system is shown in Figure 4.22 (c).

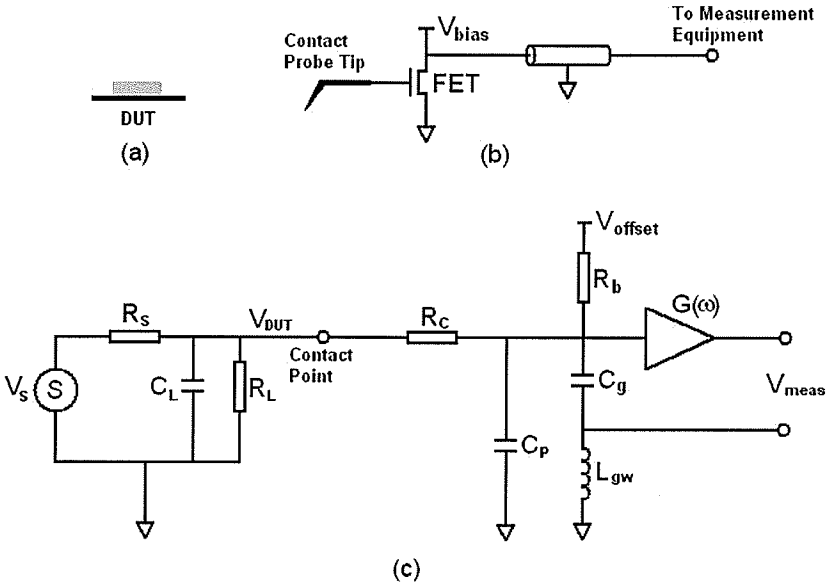

Figure 4.22 Active contact probe diagram. (a) device under test, (b) the probe implementation, and (c) equivalent circuit.

Where R_S, C_L, and R_L are test circuit's internal loads, V_{DUT} is the signal to be measured, R_c is the contact resistance between the probe tip and test point, C_p is the parasitic capacitance of the probe, R_b is a very large resistor to control the buffer gate charging, C_g is the gate capacitance of the FET, L_{gw} is the ground wire parasitic inductance, $G(\omega)$ is the amplifier's frequency response, and V_{meas} is the measured voltage. The measured voltage can be given by:

$$V_{Meas.} = V_{DUT}\left(\frac{G(\omega)}{(1+j\omega C_p R_c)(1-\omega^2 C_g L_{gw})+j\omega C_g R_c}\right) \tag{4.21}$$

Typical values, same as in last section, of these parasitic parameters for the AFM-based contact probe system are: C_p=0.1pF, and L_{gw}=50nH. Z_0 is always 50Ω for impedance match at high frequency measurement. C_g=0.05pF, a typical value of a buffer FET [2].

There are two cutoff frequencies of this active probing system, f_{c1} and f_{c2}, and they can be expressed and estimated as:

$$f_{C1} = \frac{1}{2\pi C_p R_c} \approx 3.2GHz \quad for \quad R_c = 50\Omega \tag{4.22}$$

$$f_{C2} = \frac{1}{2\pi\sqrt{C_g L_{gw}}} \approx 3.0GHz \tag{4.23}$$

According to Equation (4.18), maintaining a smaller contact resistance is very important to the active probe measurement bandwidth. If R_c equals to 1kΩ (It happens when probe tip wears), the probe bandwidth will be reduced to 160MHz.

Unlike the passive probe, the extra load experienced by the DUT is mainly the capacitive load from C_g and C_p. The pure resistive load R_b is large and can be as large as 10MΩ.

Chapter 5

Measurements using EFM and AFM Probing Systems

IC internal node signal measurement techniques and their laboratory tests have been extensively studied previously in [39]-[45]. The work of this report was mainly focused on applications of EFM and AFM probing systems in more practical measurements. Several commercial chips were studied, and state-of-art IC fabrication processes were characterized by the probing systems. This chapter presents measurement results and analyses, some of them have been published in [46]-[49].

5.1 Typical measurement setup

All tests to be reported in this chapter were performed with a similar measurement setup configuration. This general test environment is illustrated in Figure 5.1. The following are descriptions of the system function blocks of this general setup, and detailed measurement parameter setup, DUT preparation, and DUT stimulus generation of individual test will be reported separately later.

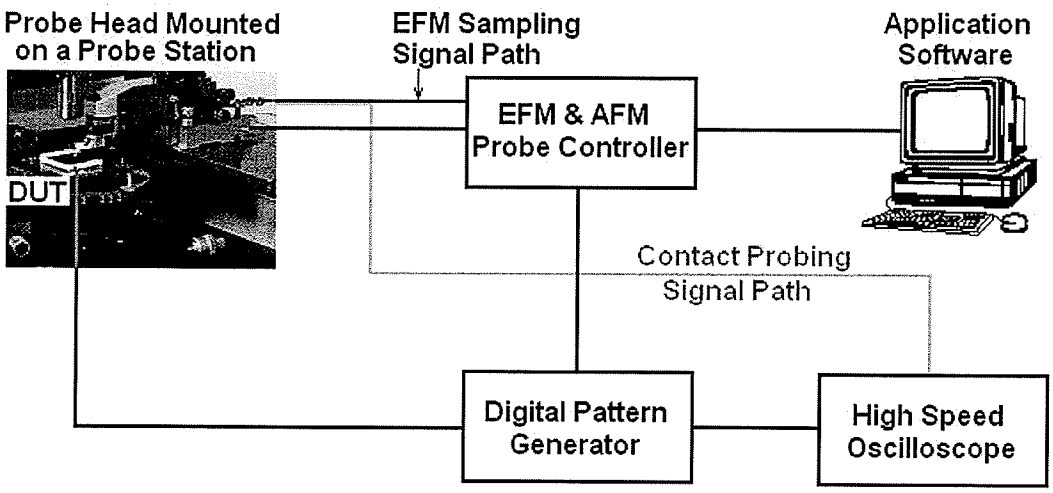

Figure 5.1 Typical measurement setup.

General test setup system function blocks are as follows:

- **Probe station.** A standard probe station was used to provide mechanically stable platform for the EFM and AFM probing systems. Probe station's optical system and position stage are also used to coarsely locate test points and help to put probe tip close to them initially.

- **EFM/AFM probe tip assembly.** Depending on the test to be performed, EFM or AFM probe tip assembly is chosen. For non-contact EFM sampling, there is only one option of probe tip assembly, which has the EFM probe tip at end of it and connect it through a 50Ω transmission lines to sampling pulse generator. For contact probing, there are two types of contact tip assemblies: passive resistor-divided probe and active high impedance probe.

- **Probe Head.** As the details of it have been presented in last chapter, probe head's capabilities can be summarized as: it is able to perform high-resolution imaging and fine positioning in a range of 40x40x40μm provided by the Piezo XYZ-actuator; the Laser cantilever deflection detection system is integrated in the probe head, and it provides the high frequency signal path for sampling pulses to

the EFM probe tip assembly or contact probing signals from the tip assembly to measurement equipment.

- **EFM and AFM probe system controller and Application Software.** This is the controlling system that integrated both EFM and AFM probing techniques. It automates most of the probing procedures through the application software.

- **Digital Pattern Generator.** A Tektronix HFS 9000 digital signal generator was used, which was able to generate signal at 680Bit/s with 200ps rising/falling times.

- **Measurement Equipment.** A Tektronix 11801B oscilloscope with SD26 sampling heads was used. It has 20GHz measurement bandwidth and 17.5ps rising/falling time specifications.

The following sections report measurement results performed on six different devices. First five tests utilized EFM sampling probe system, and last one was measured using AFM contact probe system.

5.2 Measurement on a 0.5μm CMOS test circuit

To evaluate the practical capabilities of the proposed EFM probing technique, measurements were performed on an inverter chain chip. The test device was fabricated in HP's 0.5μm CMOS technology via Canadian Microelectronics Corporation (CMC). A microphotograph and equivalent schematic of the circuit is shown in Figure 5.2.

The test structure consists of four rows of smallest standard cell inverters, and some15x15μm test pads were inserted in various locations, as shown in Figure 5.2, between inverters. First three rows' test pads have 10x10μm un-passivated openings, and the last row's test pads are passivated. The chip is operated at 3.3V and circuit stimulus signals were provided through the input pad.

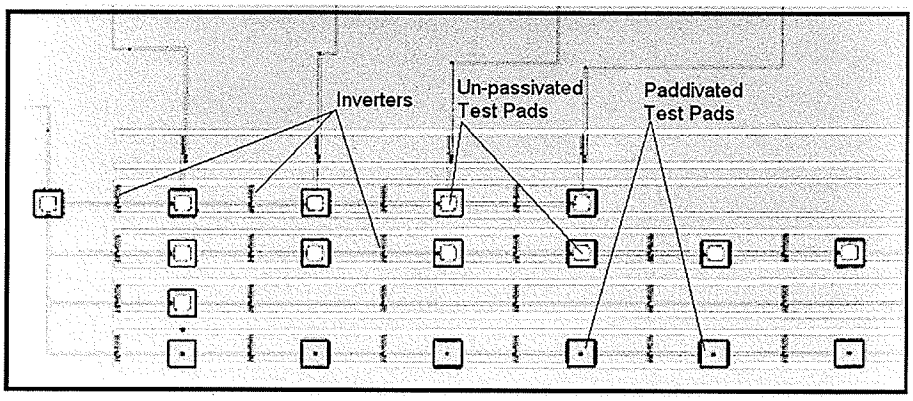

(a)

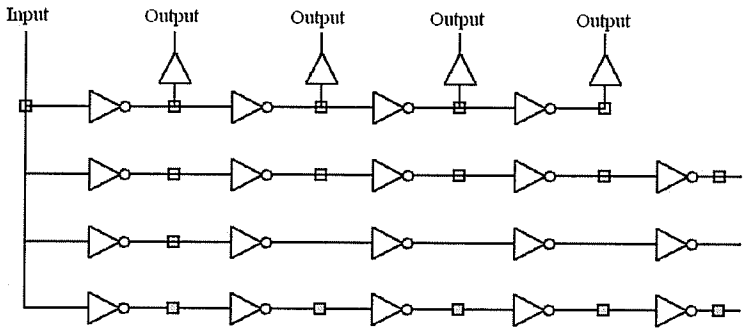

(b)

Figure 5.2 (a) Microphotograph of the CMOS inverter chain. (b) The inverter chain circuit schematic.

Several EFM probing measurements were performed on this device and we report them as follows:

5.2.1 100Mb/s data waveform probing

A 8-bit digital pattern at 100Mb/s [01011010] was applied to the input pin, and EFM probing was performed over a 10x10μm un-passivated pad. The following is the EFM measurement parameter setting: the sampling pulse is 1ns wide and 2.6V square-wave function; waveform is sampled at 200ps time intervals; single data acquisition time is 200ms; and tip to surface separation is 200nm. Figure 5.3 exhibits the measured wave-form using EFM probe and the data input waveform. By comparing measured waveform with input waveform, it is obvious that the EFM probing system is capable to extract

digital data bit information at this speed and logic swings. Using the data measured by EFM, we calculated that the EFM system RMS noise for this measurement is 0.07 ± 0.02V. Definitely, the EFM system is able to sampling signals at even higher data rates and lower logic swings.

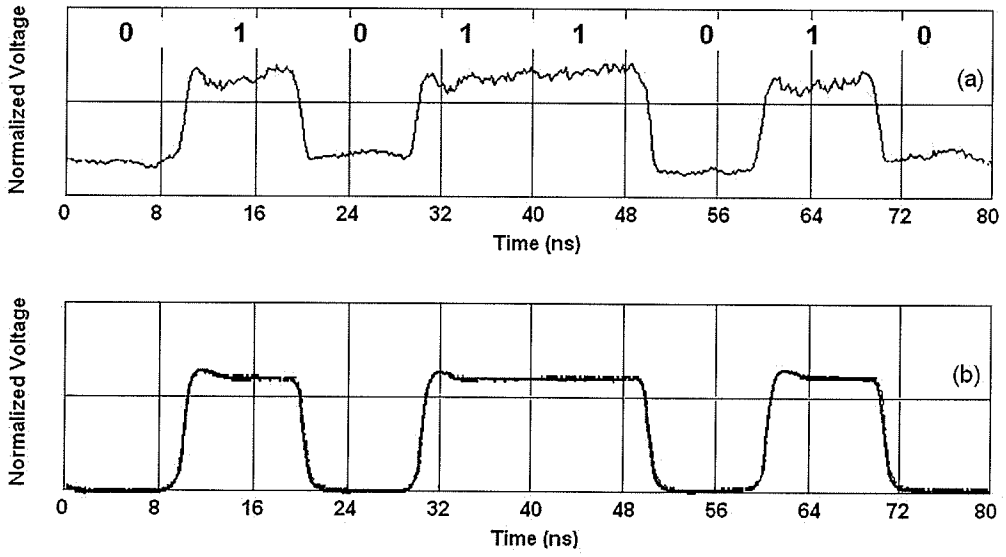

Figure 5.3 (a) 100M/s data signal measurement on 0.5μm CMOS inverter chain. (b) The 100M/s input waveform.

5.2.2 EFM probing through passivation layer

The EFM system was also used to measure signal through the passivation layer, which is the top insolating layer deposited during the CMOS process. The passivation layer over metal3 of this CMOS process is Nitride with a thickness of 0.5μm. As it is based on non-contact capacitive interaction between the probing tip and the test conductor, the EFM system is able to probe signals through passivation. A stimulus of a 100MHz clock signal was applied to the inverter chain. EFM sampling pulse was set at 1ns and 2.6V, and waveforms were sampled at 100ps step interval and 200ms single data acquisition time. Resulting waveforms over both passivated and un-passivated pads are shown in Figure 5.4. The tip-to-surface separation is set at 0.3μm in the EFM probing system, so the separation from the probe tip over a passivation layer to test conductor is about 0.8μm

and it is 0.5μm larger the distance when the probe tip is over an un-passivated test point. As the electrostatic force is proportional to the capacitance gradient, which is changing inversely with the power of two of the tip-to-surface separation, the EFM probing system signal-to-noise ratio will be reduced as the separation increases. It can be seen in Figure 5.4 that higher RMS noise on the waveform sampled over passivation layer than the one over un-passivated pad. Theoretically, the passivation layer also increases the dielectric constant of the capacitance and thus increases the capacitance, however its contribution is much smaller than the separation factor. This relation can also be seen in following sample equation of a capacitor formed by two parallel conducting plates:

$$C = \frac{\varepsilon A}{z} \quad then \quad \frac{\partial C}{\partial z} = -\frac{\varepsilon A}{z^2} \tag{5.1}$$

where ε is the dielectric constant of material between the two plates, A is the area of a plate, and z is the separation between the two plates. We can see that the capacitance gradient, $\frac{\partial C}{\partial z}$ which is proportional to electrostatic force in an EFM system, changes linearly with dielectric constant but exponentially with the separation.

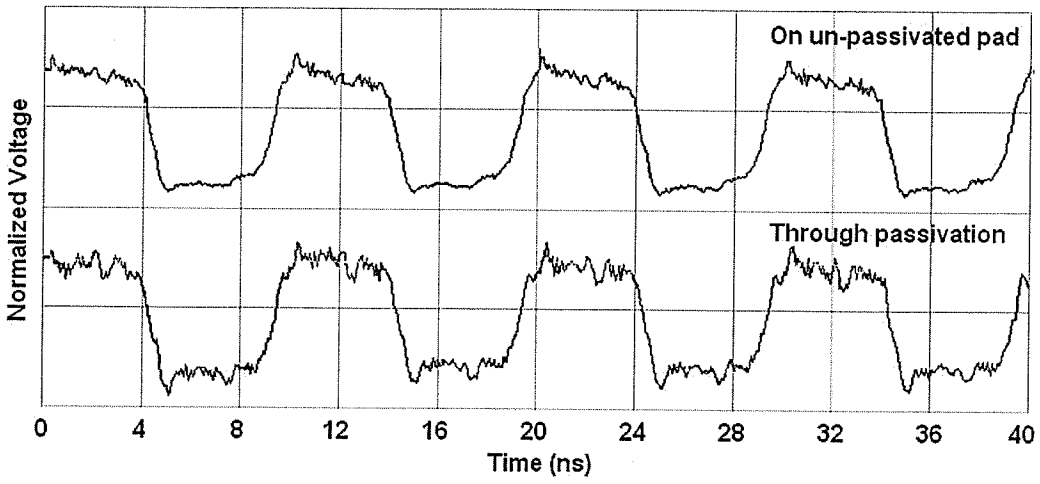

Figure 5.4 Waveforms of 100MHz clock signals measurement over un-passivated pad and through passivation.

The EFM system can sample signal waveforms even through insolating passivation layer due to the nature of its electrostatic interaction between the probe and the circuit conductors. As the passivation layer prevents the tip to be placed closer to the test conductor, the system signal-to-noise is higher when measurements are performed over passivation.

5.2.3 Duty cycle test

Due to the complexity of today's digital ICs, some digital events may only happen once in a few hundreds even few thousands of clock cycles. Testing such digital events requires measurements of long duty cycle repetitive digital patterns.

A 100-to-1 duty cycle test was performed by the EFM system on the inverter chain sample. The input signal is a 100-bit repetitive digital data at 125Mbit/s data rate (8ns clock period). Except only one data bit is asserted to logic "0" (0V), all other bits are set to logic "1" (3.3V). This signal was sampled by the EFM probing system with a sampling pulse of 1ns and 2.6V, a sampling step interval of 500ps, and single point data acquisition time of 200ms. For the full waveform, which is 800ns in time, sampling was finished in 320 seconds. The measured waveform is exhibited in Figure 5.5.

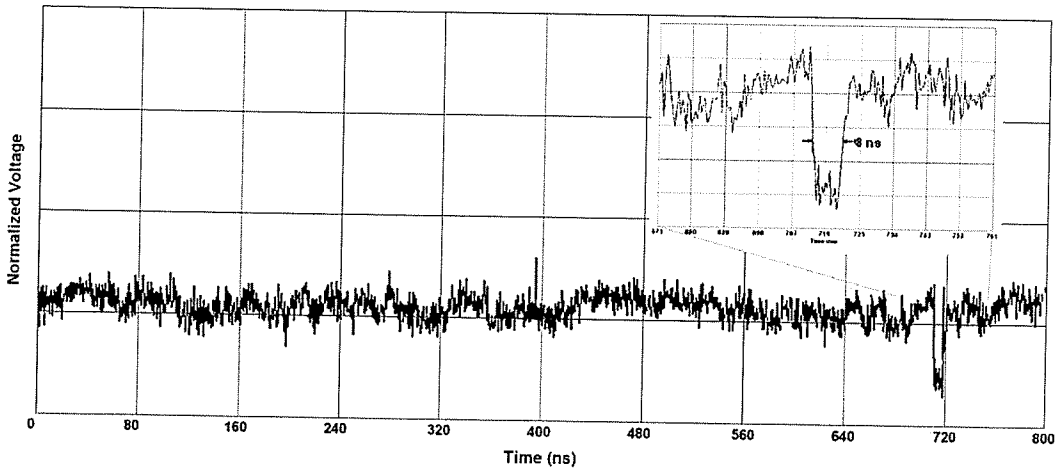

Figure 5.5 A 100-to-1 duty cycle test performed by the EFM sampling probe.

Clearly, the logic "0" bit was detected by the EFM measurement, which is located at 712ns. A 90ns zoom-in picture is also seen in Figure 5.5, which gives more detailed

waveform information of the logic bit. The RMS noise of this measurement was calculated out at 0.28 ± 0.05V for 3.3V logic swing. The low frequency system noise, which is represented by the envelope of the measured waveform in Figure 5.5, can be effectively reduced by multi-loop test features of the application software, however with the compromise of the longer acquisition time. A theoretical voltage sensitivity study of the same type EFM cantilever was perform in [4] based on the cantilever thermal noise, and RMS noise was estimated at $20mV/\sqrt{Hz}$ in condition of a 0.75V and 140ps sampling pulse and T=8ns. Using test parameter in this measurement and comparing with the study result, we can get that the EFM system thermal RMS noise for this test should be around $80mV/\sqrt{Hz}$. 100ms was the lock-in amplifier measurement time for one single data point, and effective bandwidth is 10Hz. Then the theoretical estimation of the system thermal noise is 253mV. Measured the RMS noise was larger as it was the overall system noise and it included other types of noise, such as vibration.

5.2.4 Propagation delay measurement

The smallest standard cell inverter's propagation delay is a key technology parameter to characterize a CMOS process. For instance, IBM specifies that this parameter is 27ps for its state-of-the-art 100nm Cu CMOS process [50]. This specification is measured internally on the inverter chain device for the HP 0.5μm CMOS process using the EFM probing system.

The tests were done on a clock signal over the test pads between every two inverters of the second inverter row of the test device. More detailed "zoom-in" measurements were performed on the same rising edge of the signal at those different locations. The rising edge were sampled by 1.2V 400ps sampling pulses, at every 20ps a step, and 500ms sampling time for single data point, and the four measured rising edges (represented by four different colored curves) are shown in Figure 5.6. The signal steps on the rising edges were related to the time unit's delay control scheme, as the time unit may switch an array of delay elements on and the other array of delay elements off in the same time and this may cause a small delay discontinuity.

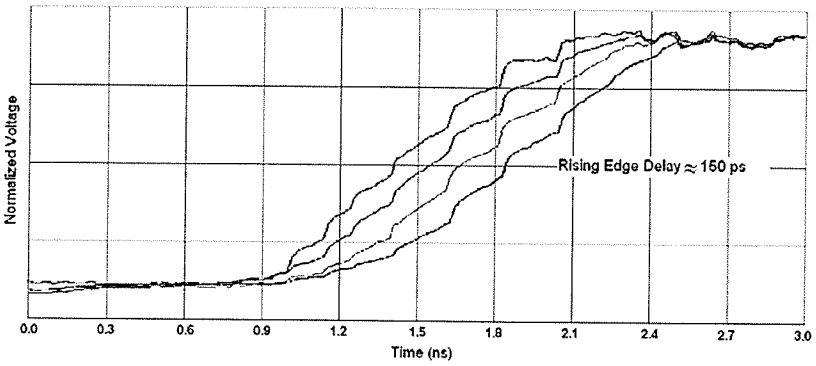

Figure 5.6 Sampling waveforms of rising edges and inverter chain delay measurement.

According to Figure 5.6, the propagation delay between two inverters is 150ps. So the smallest standard cell inverter's propagation delay is 75ps, which is consistent with analog simulation result using Cadence SpectreS simulator and process data provided by HP, which is specified at 88ps [51].

5.3 TI DSP TMS320C30 Clock distribution tree measurement

A TI TMS320C30 DSP, which is inserted on a commercial of-the-shelf evaluation board from Texas Instruments, was also tested by the EFM probing system. The board was powered and controlled through a PCI bus cable which extends out from a PC and no special fixture and stimulus are needed.

Internal signal measurements were performed on the clock distribution tree of this TI DSP chip. A clock distribution tree likes the "nerve system" of a digital chip. It provides trigger signals of all the sequential logic elements of on the digital chip, and all digital data vectors' computing operations are timed by this clock. So the timing information of the clock distribution tree is of utmost important to a digital chip.

The IT DSP, as shown in Figure 5.7, takes a single 30MHz clock input from a crystal oscillator, and converts it into two 180-degree-out-of-phase 15MHz clock signals. These two signals are distributed all over the chips, and there are many clock leaf drivers con-

necting to the two lines and driving local circuit elements. The following points of this clock tree were tested by the EFM probing system: the clock trace right after the clock input pad, the clock lines after first stage clock buffers, and points before and after one local clock buffers.

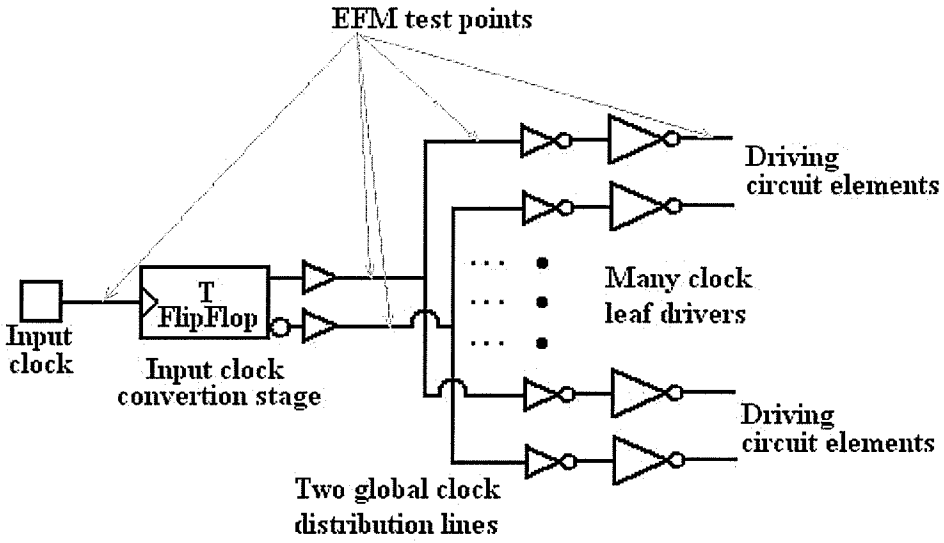

Figure 5.7 TI TMS320C30 DSP clock distribution tree circuit schematic.

AFM images were also scanned by the probe system to aid the probe positioning. Figure 5.8 exhibits the images of the test area including the input clock trace.

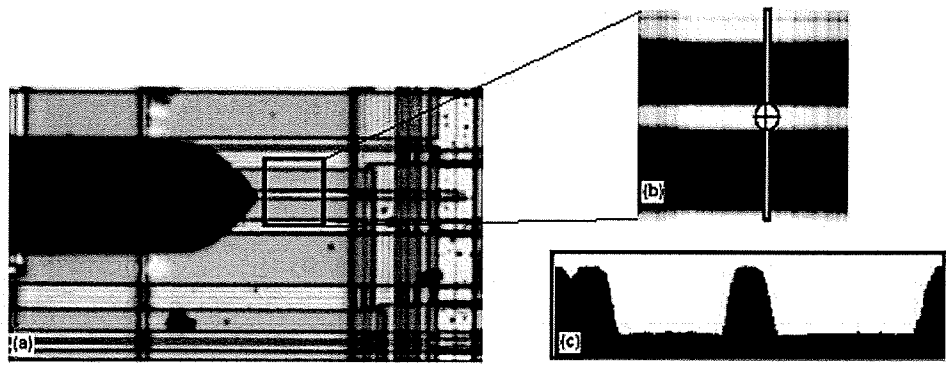

Figure 5.8 (a) Input clock trace under EFM probe, (b) 40x40um AFM image of the area over the input clock trace, and (c) A cross section of the image.

Figure 5.8 (a) shows the microscope image of the EFM probe seating over the clock trace right after a touchdown surface finding procedure was performed, Figure 5.8 (b) is the high-resolution image token using the probe's AFM scanning operation, and Figure 5.8 (c) is a cross section of the AFM image. As the clock line (indicated by a cross in Figure 5.8) is wide enough to resolve it on the 40x40um image, no zoom-in AFM image was taken. The input clock trace width is measured at 5 um from the cross section picture.

All EFM measurements were performed over the passivation layer with 2.6V and 1.3ns sampling pulses. Figure 5.9 shows the clock signals measured at input trace and the two points after the input clock converting stage.

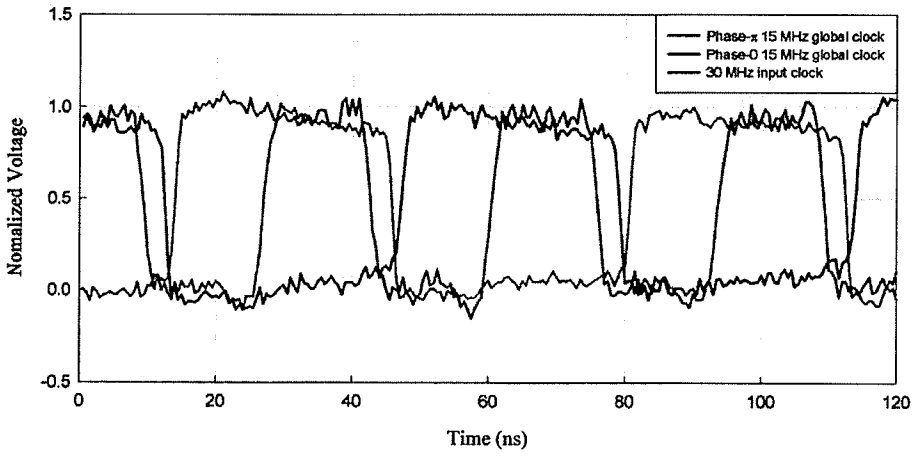

Figure 5.9 Measurement of clock input and on chip out-of-phase clock signals of a TI TMS320C30 DSP.

The red waveform is the input 30MHz clock. The green and blue waveforms are the two out-of-phase clock signals. Not only was the signal converting operation verified through this measurement, but also the converting stage propagation delays were resolved by comparing the transition edges. The delays are 3.5ns and 5.9ns from the input to the two-out-of-the-phase output ports. Larger delay at one output is due to the signal inverting inside the stage.

Figure 5.10 shows a microphotograph of two leaf clock drivers of the clock tree on the TI DSP. The sizes of them are much larger then the logic circuit elements shown in the same figures. This suggests that the clock tree leaf driving buffers may consist of more

inverter stages (4 or 6 stages) to increase the drivability. A clock leaf buffer usually drives a block area on the chip and it may contain a substantial amount of circuit element. The capacitive load of the clock leaf buffer can be large which requires large drivability.

EFM tests were taken before and after one of the buffer as indicated in Figure 5.10. The signal is basically the one 15MHz clock. EFM probe measured waveforms were given in Figure 5.11.

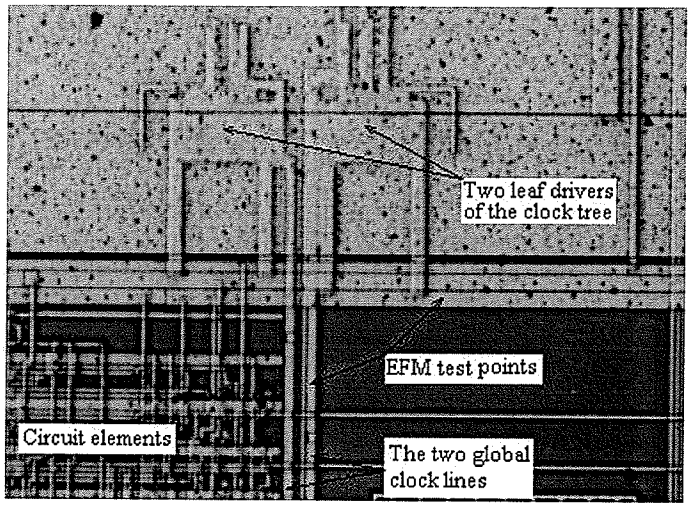

Figure 5.10 Microphotograph of two clock driver buffers of the clock distribution tree in a TI TMS320C30 DSP.

Figure 5.11 (a) shows the input signal of the buffer in red waveform and output in blue. They were measured at 0.5ns step interval. In order to observe the propagation delay of the buffer, detailed "zoom-in" measurements were taken at 50ps a step on the falling edges. It results that there is a 0.8ns propagation delay for the leaf clock buffers.

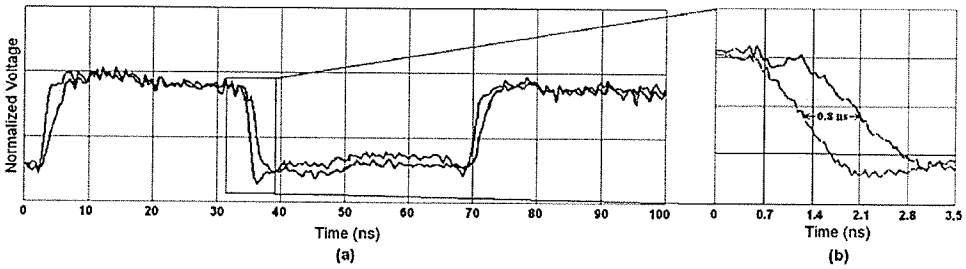

Figure 5.11 Delay measurement of a TI TMS320C30 DSP clock tree buffers.

The tests on this IT DSP demonstrate that a fairly large digital chip's clock distribution network were studied by the EFM probing system, various driving stages' timing information were obtained with 50ps resolution, and the measurements were through the passivation layer and non-invasive too.

5.4 Backside Probing

Backside diagnostic techniques are important because many IC manufacturers, especially the high performance microprocessors vendors, have adopted flip-chip packaging in the past several years. In a flip-chip configuration, as shown in Figure 5.12, a silicon die is flipped upside-down and bonded directly to a substrate. Flip-chip technology has the advantage of a superior electrical performance. It reduces parasitic effects of chip bonding wires, and it helps address the power- and clock-distribution problems by allowing bonding pads to be placed at any position on the chip instead of making all I/O connections on the die boundary. However it also makes the die un-accessible to probe from circuit side, and backside probing has to be used in flip-chip mounted IC failure analysis.

Non-contact EFM probing technique was also used for measuring high-frequency voltage waveforms from the backside of flip-chip mounted integrated circuits. Test results have been published in [48], and this section reports them.

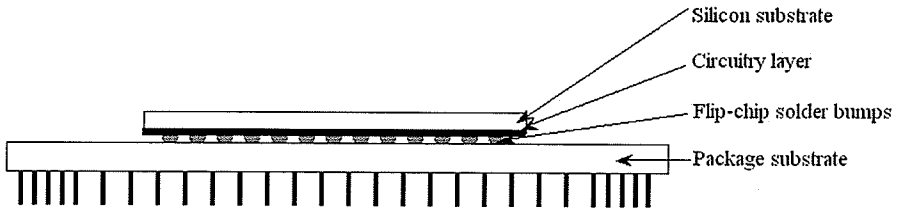

Figure 5.12 A diagram of flip-chip mounting configuration.

The backside samples were ring oscillators prepared as part of the development of a state-of-the-art microprocessor. Figure 5.13 is shown a photograph the test setup, where

the EFM probe seats above the flip chip sample. The probe is intended to operate on a standard probe station configuration.

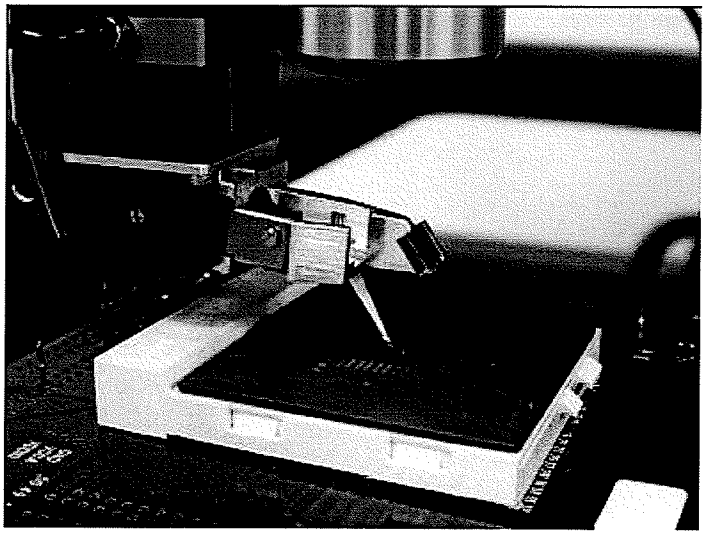

Figure 5.13 Non-contact EFM sampling probe mounted above a backside test sample.

Normally, a silicon die substrate has a thickness of 250-500μm. Several steps have taken to prepared backside EFM probe samples. A cross section of a backside test sample is illustrated in Figure 5.14, and backside probe sample preparation steps are:

- Silicon dies was mechanically thinning down to thickness of about 100-150μm globally.

- A Focus Ion Beam (FIB) is used to further thin the test area to 10-15μm from the circuit active layer. A FIB tool operates in vacuum, and it takes charged gallium ions from a field emission liquid metal ion source, focuses them into a beam through electromagnetic/electrostatic lenses, and then scans across small areas of the sample using deflection plates or scan coils. Since gallium ions are heavy ions comparing to electrons, a FIB's ion beam mills the sample surface as it scans it. A FIB tool is used to precisely mill silicon substrate layer by layer in our sample preparation. On our test samples, 150x150μm trenches are made over the circuitries we are interested.

- Small test holes are opened by the FIB above the test points interested. FIB is also capable of making fine cuts on silicon with accuracy as high as 0.01μm. In our case, several 5x5μm, 10x10μm, and 15x15μm square test holes were made, shown in Figure 5.15.

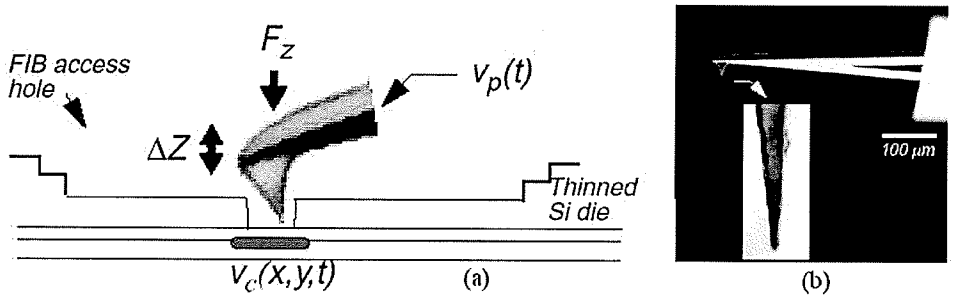

Figure 5.14 (a) Micro-machined probe with <50nm radius tip at the apex, (b) The probe is placed in a FIB-milled access hole from the chip backside.

Figure 5.15 exhibits the EFM probe seating in the backside access trench of the test sample, and a higher magnification micrograph of the FIB access holes. Figure 5.15 (c) is a 40x40μm AFM image of the area with two 5x5μm FIB access holes. EFM probe positioning was guided by this image.

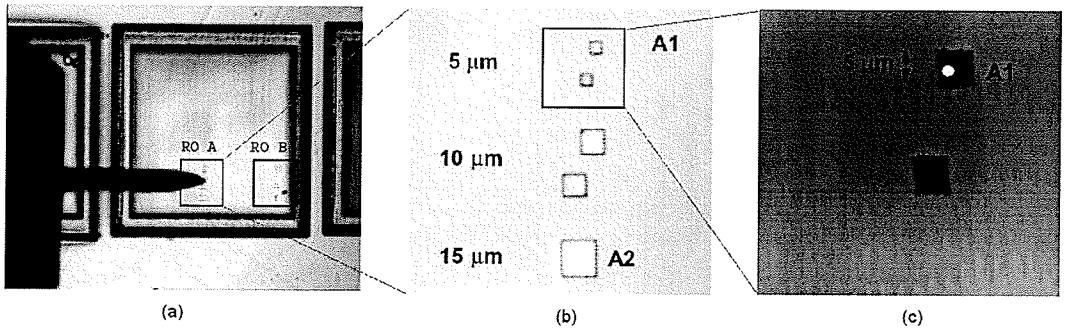

Figure 5.15 (a) Micrograph of probe in a backside access hole, (b) Higher magnification micrograph of the FIB access holes for the ring oscillator, and (c) AFM mode image of 5x5μm FIB access holes.

As the test structure is a ring oscillator, the EFM measured waveform, as shown in Figure 5.16, is a clock signal with a period of 6.1ns for this ring oscillator.

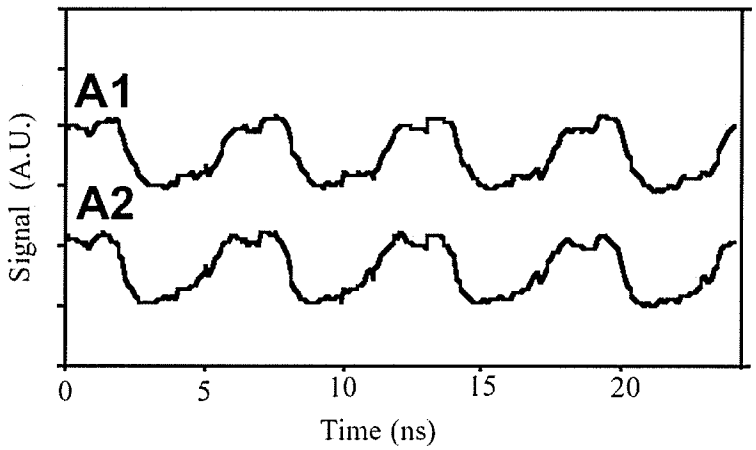

Figure 5.16 Ring oscillator waveforms taken using EFM probing system through backside access holes.

5.5 AFM Sub-Micron Contact Probing measurement

This section reports the AFM sub-micron imaging and computer-controlled probe positioning abilities of the AFM-based contact probing system and the real-time electrical measurement realized by the contact probing assemblies. Measurement results was also published in [47] and [49].

The test structure To demonstrate the AFM sub-micron imaging and computer-controlled probe positioning abilities, a group of three 0.5μm interconnect lines with 0.5μm separation test structure was used. For comparison, Figure 5.17 (a) shows a photomicrograph of a typical etched-wire probe with a tip of 1μm over the 0.5μm interconnect lines. As one can easily notice, using even an etched wire probe of very small diameter, it is difficult to obtain a contact with only one of the metal traces. One the other hand, Figure 5.17 (b) shows the scanned AFM image of the same corner of the test structure. Note that at the AFM resolution, one can clearly see the three 0.5μm interconnect lines, and even sub-0.1μm surface details.

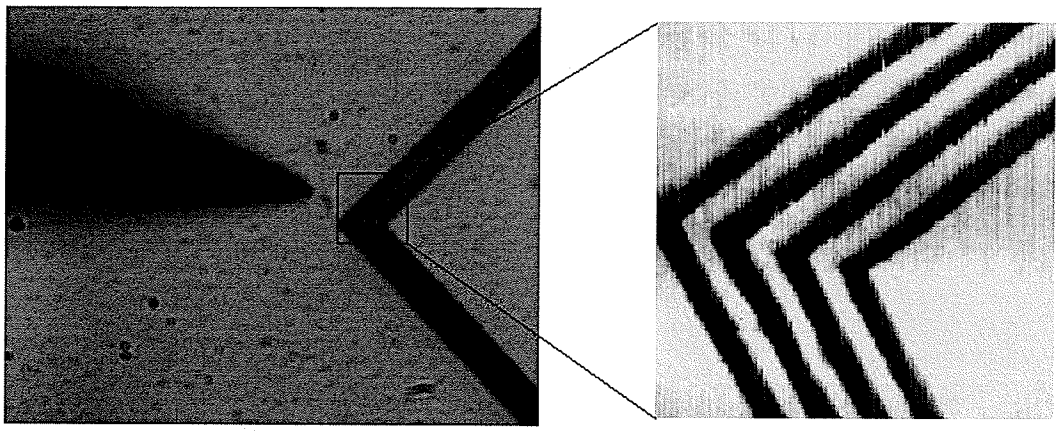

Figure 5.17 Typical 1μm etched needle probe near three 0.5μm interconnect lines.

A high frequency signal test was performed by an AFM-based passive contact probe tip assembly on a 1mm wide 50Ω-transmission line structure. Measurement results are shown in Figure 5.18. In this test, a 120ps risetime pulse was the stimulus signal. The probe was a 40-to-1 (using a 1950Ω divider-resistor) passive contact tip assembly. The probe output and the test structure output were all connected to a Tektronix 11801B high frequency oscilloscope (20GHz bandwidth, 17.5ps rising/falling times).

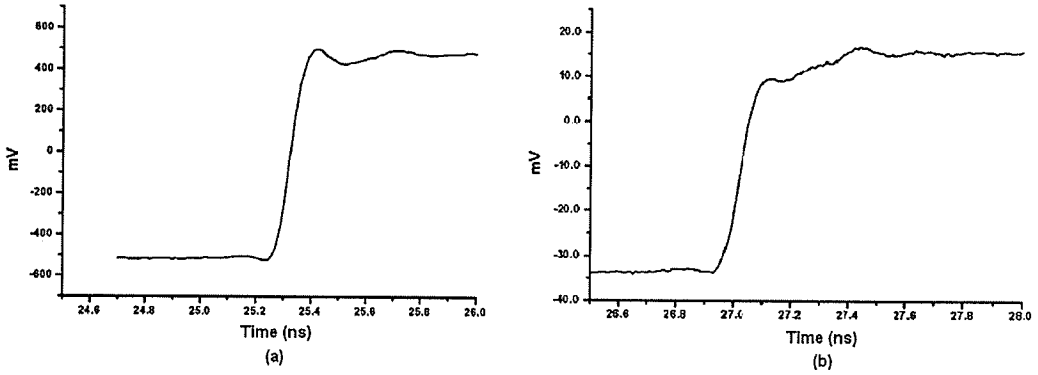

Figure 5.18 120ps risetime edge measured by (a) Tektronix oscilloscope, (b) AFM-based passive contact probe.

Figure 5.18 (a) shows the rising edge measured directly by the oscilloscope at the output of the test structure. Figure 5.18 (a) shows the same rising edge measured by the oscillo-

scope through the contact passive tip assembly. These results clearly show that the risetime measured using AFM-based passive contact probe is equivalent to that of the stimulus signal.

Another test results are shown in Figure 5.19. In this test, a 200Mbit/s 8-bit pattern was the stimulus signal. A active tip assembly was used in the measurement, and a Tektronix SD14 active probe was also used to probe the signal for comparison. Figure 5.19 (a) shows the waveform measured by the Tektronix probe, and Figure 5.19 (b) is the waveform probed by the active contact tip assembly. Clearly, the active tip assembly has a comparable bandwidth with the Tektronix active probe.

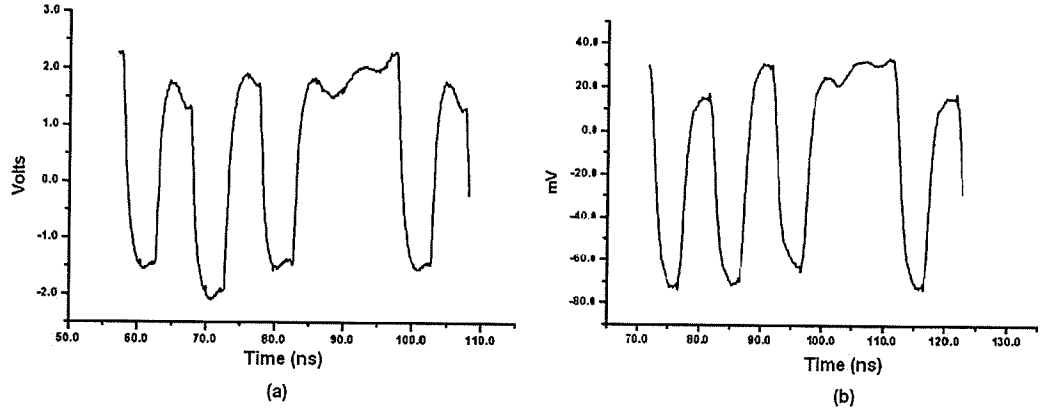

Figure 5.19 200Mb/s signals measured by (a) Tektronix active probe, (b) AFM-based active contact probe.

AFM-based contact probe applications to more practical measurements have also been reported in [52] and [53].

Chapter 6

Conclusions and Future Work Suggestions

6.1 Conclusions

Two IC internal signal measurement techniques have been presented. They are the amplitude modulation high-speed EFM sampling technique, and AFM-based sub-micron contact probing technique. Theoretical analysis reviews that EFM sampling is a non-invasive, high spatial resolution, and high bandwidth measurement technique.

Both techniques has been implemented and integrated into one practical probing system which can retrofit and work with a typical probe station. Probe tip assemblies for EFM sampling, and passive and active contact probing techniques have been developed.

Internal signal measurements have been performed on an inverter chain structure fabricated in HP's 0.5μm CMOS technology and on a TI TMS320C30 DSP which is a commercial off-the-shelf device. The test results demonstrate that the EFM sampling technique is able to verify various digital signal properties on practical devices, such as: data pattern extraction, timing information of logic state switching, signal propagation delay measurement with below ten picosecond resolution, and long duty cycle digital vector measurement. The EFM sampling technique is also capable of signal measurement through chip passivation layer.

Backside probing for flip-chip configuration devices is tested using the EFM measurement system, and simple ring oscillator clock signal was extracted. More experiments have to be done to explore the applications of EFM sampling technique on backside measurement.

AFM-based contact probing system has been demonstrated that it is capable of 100nm resolution surface imaging and precisely controlled probe positioning. Both passive and active contact tip assemblies have compatible measurement bandwidth with the traditional contact probes.

6.2 Future Suggestions

6.2.1 Piezo-resistive deflection sensor

One shortcoming of the Laser deflection detection system is that there is a mirror located in front of cantilever tip (As shown in Figure 4.11). This configuration may be an obstacle for access deep probe card opening, and prevent its application of multi-probing. There is always a desire to using several probes simultaneously for certain devices failure analysis. One possible solution is to use piezo-resistive deflection sensor instead of Laser beam bounce system. As shown in Figure 6.1, using modern MEMS (Microelectromechanical System) technology, a piezo-resistive resistor can be implanted right in the cantilever. As a piezo resistor changes resistance when it experiences stress, it will sense the cantilever deflection which creates stress over the cantilever. Such piezo resistive MEMS system has been applied to some of pressure sensor developments.

The advantage of the piezo-resistive deflection sensor is obvious. All the optical parts are not needed including the front mirror. This will dramatically reduce the size of the probe head and simplify the control electronics, as the Laser beam bounce system takes the most of the probe head space and lots hardware devoted to the detection system's adjustment and calibration.

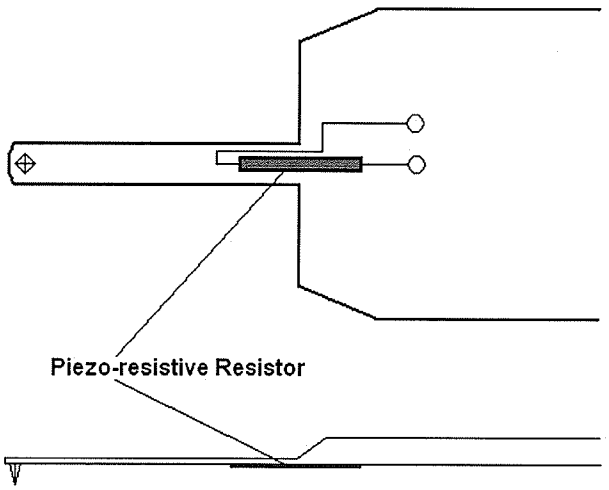

Figure 6.1 A piezo-resistive resistor is implanted in a cantilever as deflection sensor.

6.2.2 Multi-channel Sampling

The proposed EFM sampling technique is using one sampling pulse within one period of a repetitive signal and the waveform can only be extracted one point a time. Theoretically, there can be multiple sampling pulses and the waveform can be built several data points a time to reduce total measurement time. Practically, it is also possible to implement a multiple pulse sampling technique with the EFM system. A multi-channel EFM sampling technique has been proposed by the researchers at University of Manitoba. As shown in Figure 6.2, there are five sampling pulses at different phase locations within a one period of a repetitive pattern. In order to distinguish the five sampling pulses' sampled data, they are modulated with different frequencies. EFM sampling technique also requires the sampling pulse to be modulated close to the cantilever resonant frequency so that to increase the detected deflection signal, so the five sampling pulses are located close to either other around the cantilever resonant frequency, as shown in the frequency-domain curve in Figure 6.2 (b). The frequency separation can be as low as 10Hz, as a lock-in amplifier used to measure a signal just at certain frequency is a very narrow band-pass flitter amplifier.

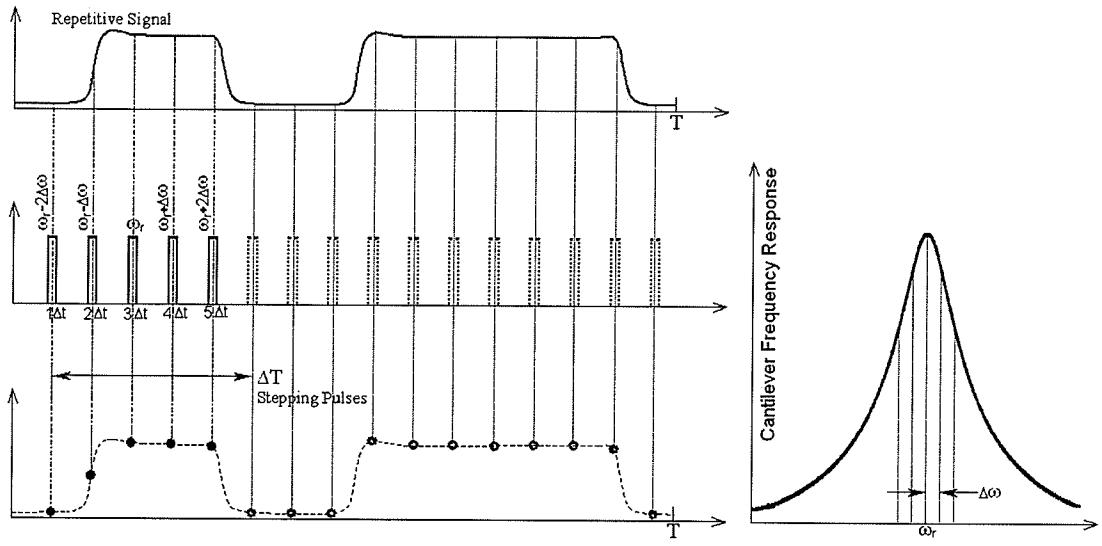

Figure 6.2 (a) Multi-channel sampling pulse timing diagram. (b) Multi-channel sampling pulse frequency domain diagram.

Future work of this technique may involve the development of hardware which is able to multiplex the modulated multi-channel sampling pulse trains into one signal so that to send it to the EFM probe. Using several lock-in amplifier instruments to measure the multi-channel data seems not a practical approach. Fortunately, modern DSP signal processing power would be sufficient enough for this job. The implementation of DSP data process of this technique would be a good development project.

References

[1] Semiconductor Industry Association, (http://www.semichips.org), "2001 International Technology Roadmap for Semiconductors (ITRS)", 2001 Edition

[2] GGB Industries Inc., (http://www.picoprobe.com).

[3] G. Rabjohn, J. Wolczanski, and R. Surridge, "High-Frequency Wafer-Probing Techniques," *Canadian Journal of Physics,* vol. 65, no.8, pp. 850-855, 1987.

[4] S. P. S. Cheung, "Electrostatic Force Sampling of Digital Waveforms Using Synchronous Time Domain Gating," M.Sc. Thesis, Dept. of Electrical and Computer Engineer, University of Manitoba, Canada, 2000.

[5] J. A. Valdmanis and G. Mourou, "subpicosecond Electro-Optic Sampling: Principles and applications," *IEEE Journal of Quantum Electronics,* vol. QE-22, no.1, pp. 69-78, 1986.

[6] John T. L. Thong, "Electron Beam Testing Technology", *Plenum Press*, pp. 1-5, 1993.

[7] W. Mertin, A. Leyk, U. Behnke, and V. Wittpahl, "Contactless GigaHertz Testing," *Proceedings of the 1998 IEEE International Test Conference*, pp. 845-852, 1998

[8] J. Fehr and E. Kubalek, "Electron Beam Test System for GHz-Waveform Measurement on Transmission Lines within MMIC," *Proceedings of the 22nd European Microwave Conference*, pp. 163-168. 1992

[9] S. Runyong, "Optical system probing flip chip from backside" *EE Times*, CMP Media Publish, vol. 9, 1998

[10] J. C. Tsang, J. A. Kash, and D. P. Vallett, "Picosecond imaging circuit analysis", *IBM Research Journal,* vol. 10, 1999

[11] J. I. Pankove, "Electroluminescence," Berlin, Springer-Verlag, pp. 31, 1977

[12] G. David, P. Bussek, A. Auer, F.J. Tegude, and D. Jager, "Electro-Optic Probing of RF Signals in Submicrometre MMIC Devices," Electronics Letters, vol. 31, no. 25, pp. 2188-2189, 7th December 1995

[13] G. Dajee, N. Goldblatt, T. Lundquist, S. Kasapi and K. Wilsher, "Practical, Non-invasive Optical Probing for Flip-Chip Devices," *IEEE International Test Conference*, pp. 433-442, 2001.

[14] G. Binnig, H. Rohrer, Ch. Gerber, and E. Weibel, "Surface studies by scanning tunneling microscopy," *Physical Review Letters,* vol. 49, no. 1, pp. 57-61, 1982.

[15] G. Binnig, C. F. Quate, and Ch. Gerber, "Atomic force microscope," *Physical Review Letters, vol. 56, no.* 9, pp. 930-933, 1986.

[16] R. C. Barrett and C. F. Quate, "Charge storage in a nitride-oxide-silicon medium by scanning capacitance microscopy," *Journal of Applied Physics,* vol. 70, no. 5, pp. 2725-2733, 1991.

[17] C. Shafai, D. J. Thomson, and M. Simard-Normandin, "Two-dimensional delineation of semiconductor doping by scanning resistance microscopy," *Journal of Vacuum Science and Technology,* vol. B12, no. 1, pp. 1-5, 1994.

[18] Y. Martin, D. Rugar, H. K. Wickramasinghe, "High-Resolution Magnetic Imaging of Domains in TbFe by Force Microscopy," *Applied Physics Letters,* vol. 52, no. 3, pp. 244-246, 1988.

[19] A. N. Campbell, E. L. Cole, B. A. Dodd, and R. E. Anderson, "Internal Current Probing of Integrated Circuits using Magnetic Force Microscopy," *IEEE International Reliability Physics Symposium,* pp. 168-177, 1993.

[20] J. E. Stern, B. D. Terris, H. J. Mamin, and D. Rugar, "Deposition and Imaging of Localized Charge on Isulator Surfaces using Force Microscope," Applied Physics letters, vol. 53, no. 26, pp. 2717-2719, 1988.

[21] Y. Huang, J. Slinkman, and C. C. Williams, "Modeling of Impurity Dopant Density Measurement in Semiconductors by Quantitative Scanning Force Microscopy," Ultramicroscopy, vol. 42-44, pp. 298-303, 1992.

[22] F. Saurenbach, and B. D. Terris, "Imaging of Ferroelectric Domain Walls by Force Microscope," Applied Physics Letters, vol. 56, no. 17, pp. 1703-1705, April 1990.

[23] M. Nonnenmacher, M. P. O'Boyle, and H. K. Wickramainghe, "Surface Investigation with a Kilvin Probe Force Microscope," Ultramicroscopy, vol. 42-44, pp. 268-273, 1992.

[24] A. D. Dimarogonas, "Vibration for Engineers," Prentice-Hall, Inc., New Jersey, USA, 1996.

[25] Molecular Devices and Tools for NanoTechnology (NT-MDT) Co., Zelenograd Research Institute of Physical Problems, 103460, Moscow, Russua, www.ntmdt.ru

[26] C. A. J. Putman, B. G. De Grooth, N. F. Van Hulst, and J. Greve, "a Detailed Analysis of the Optical Beam Deflection Technique for use in Atomic Force Microscopy," *Journal of Applied Physics*, vol. 72, no. 1, pp.6-12, 1992.

[27] J. M. R. Weaver and D. W. Abraham, "High Resolution Atomic Force Microscopy Potentiometry," *Journal of Vacuum Science and Technology B,* vol. 9, no. 3, pp. 1559-1567, 1991.

[28] A. S. Hou, F. Ho, and D. M. Bloom, "Picosecond Electrical Sampling Using a Scanning Force Microscope," Electronics Letters, vol. 28, no. 25, pp. 2302-2303, 1992.

[29] G. E Bridges, R. A. Said, and D. J. Thomson, "Heterodyne Electrostatic Force Microscopy for Non-Contact High Frequency Integrated Circuit Measurement," *Electronic Letters,* vol. 29, no. 16, pp.1448-1449, 1993.

[30] A. S. Hou, B. A. Nechay, F. Ho, and D. M. Bloom, "Scanning Probe Microscopy for Testing Ultrafast Electronic Devices," *Optical and Quantum Elec*tronics, vol. 28, no. 7, pp. 819-841, July 1996.

[31] R. A. Said, "Scanning Force Potentiometry Techniques For Semiconductor Circuit Characterization," Ph.D. Thesis, Dept. of Electrical and Computer Engineer, University of Manitoba, Canada, 1995

[32] G. E. Bridges and D. J. Thomson, "High-frequency circuit characterization using the AFM as a reactive near-field probe," *Ultramicroscopy,* vol. 42: 321-328 (1992).

[33] D. Noruttun, "Non-contact Internal Probing of High Speed Microelectronic Circuits Using Electrostatic Force Microscopy," M.Sc. Thesis, Dept. of Electrical and Computer Engineer, University of Manitoba, Canada, 1997.

[34] Lecroy Co., Chestnut Ridge, New York, USA, www.lecroy.com.

[35] G. D. Cormack and A. P. Sabharwal, "Picosecond Pulse Generator using Delay Lines." *IEEE Transactions on Instrumentation and Measurements*, vol 42, no. 5, pp. 947-948, 1993.

[36] DG535 SRD module, Stanford Research Systems, Inc., www.srsys.com.

[37] "AFM Real-Time Prober," MFI Technologies, Inc.

[38] C. S. Walker, "Capacitance, Inductance, and Crosstalk Analysis," Artech House, Inc., Norwood, MA, USA, 1990.

[39] R. A. Said, "Scanning Force Potentiometry Techniques For Semiconductor Circuit Characterization," Ph.D. Thesis, Dept. of Electrical and Computer Engineer, University of Manitoba, Canada, 1995

[40] G. E Bridges, R. A. Said, and D. J. Thomson, "Heterodyne Electrostatic Force Microscopy for Non-Contact High Frequency Integrated Circuit Measurement," *Electronic Letters,* vol. 29, no. 16, pp.1448-1449, 1993.

[41] R. A. Said, G. E Bridges, and D. J. Thomson, "Scanned Electrostatic Force Microscope for Noninvasive High Frequency Potential Measurement," *Applied Physics Letters,* vol. 64, no. 11, pp.1442-1444, 1994.

[42] G. E Bridges, R. A. Said, M. Mitall, and D. J. Thomson, "Sampled Waveform Measurement in Integrated Circuits Using Heterodyne Electrostatic Force Microscopy," *Reviews of Scientific Instrument*, vol. 65, no. 11, pp.3378-3381, 1994.

[43] G. E Bridges, R. A. Said, and D. J. Thomson, "Heterodyne Electrostatic Pattern Extraction in Digital Integrated Circuits Using Electrostatic Force Microscopy," *Journal of Vacuum Science Technology B,* vol. 13, pp.1375-1379, 1995.

[44] D. Noruttun, "Non-contact Internal Probing of High Speed Microelectronic Circuits Using Electrostatic Force Microscopy," M.Sc. Thesis, Dept. of Electrical and Computer Engineer, University of Manitoba, Canada, 1997

[45] G. E Bridges, D. Noruttun, R. A. Said, D. J. Thomson, T. Lam, and R. Qi, "Non-Contact Probing of High Speed Microelectronics Using Electrostatic Force Saming," *Journal of Vacuum Science Technology A,* vol. 16, no. 2, pp.830-833, 1998.

[46] G. E Bridges, D. J. Thomson, and R. Qi, "Non-Contact Probing of Integrated Circuits Using Electrostatic Force Sampling," *Proceedings from the 24th International Symposium for Testing and Failure Analysis,* Dallas, Texas, USA, Nov. 1998.

[47] K. Krieg, R. Qi, D. J. Thomson, and G. E Bridges, "Electrical Probing and Surface Imaging of Deep Sub-Micron Integrated Circuits," *Proceedings from the 25th In-*

ternational Symposium for Testing and Failure Analysis, Santa Clara, California, USA, Nov. 1999.

[48] R. Qi, D. J. Thomson, and G. E Bridges, "Backside Probing of Flip-Chip Circuits Using Electrostatic Force Sampling," *Proceedings of International Reliability Physics Symposium,* Dallas, Texas, USA, April 1998.

[49] K. Krieg, R. Qi, D. J. Thomson, and G. E Bridges, "Electrical Probing of Deep Sub-Micron ICs Using Scanning Probes," *Proceedings of International Reliability Physics Symposium,* San Jose, California, USA, April 2000.

[50] "IBM Foundry Service: Key Technology Specifications for CMOS and RF CMOS processes," http://www-3.ibm.com/chips/services/foundry/

[51] "CMOS14TA/B Design Reference Manual," Hewlett Packard, 1995.

[52] T. Kane, M. Cambra, M. Tenney, P. McGinnis, A. Domenicucci, Y. Wang, and D. Falcon, "Characterization and Isolation Techniques in Silicon on Insulator Technology Microprocessor Designs," *Proceedings from the 26th International Symposium for Testing and Failure Analysis,* Bellevue, WA, USA, Nov. 2000.

[53] T. Kane, P. McGinnis, and B. Engel, "Electrical Characterization of Circuits with Low K Dielectric Films and Copper Interconnects," *Proceedings from the 27th International Symposium for Testing and Failure Analysis,* Santa Clara, California, USA, Nov. 2001.